

SMALL ANGLE SCATTERING OF LARGE PROTEIN UNITS UNDER
OSMOTIC STRESS

A Dissertation

Submitted to the Faculty

of

Purdue University

by

Luis A. Palacio

In Partial Fulfillment of the

Requirements for the Degree

of

Doctor of Philosophy

May 2020

Purdue University

Indianapolis, Indiana

**THE PURDUE UNIVERSITY GRADUATE SCHOOL
STATEMENT OF DISSERTATION APPROVAL**

Dr. Horia I. Petrache, Chair

Department of Physics, School of Science

Dr. Ruihua Cheng

Department of Physics, School of Science

Dr. Yogesh N. Joglekar

Department of Physics, School of Science

Dr. Jing Liu

Department of Physics, School of Science

Dr. Stephen R. Wassall

Department of Physics, School of Science

Approved by:

Dr. Ricardo Decca

Head of the School Graduate Program

Dedicated to my parents, my family, and friends who have supported and encouraged me in this endeavor; and to Philip Gurnev for initial measurements that lead to this investigation, for taking the time to welcome me into the field of biophysics and for taking the time to provide coaching, training, and mentoring.

ACKNOWLEDGMENTS

Thanks to the IU Research Investment Fund, the NSF GK-12 Fellowship (NSF-DGE # 0742475 Grant), the Alpha-1 Foundation, and Health & Science Innovations for partially funding this project.

Special thanks to Dr. Horia I. Petrache (Dept. of Physics, IUPUI) for all of his advice, help, coaching, and support that led to the development and conclusion of this research project.

Thanks to Dr. Christopher B. Stanley (Biology and Soft Matter Division, Oak Ridge National Laboratory), Dr. Soenke Seifert (Chemical and Materials Science, X-ray Science Division, APS, Argonne National Laboratory), Dr. Ann Kimble-Hill (IU School of Medicine), Dr. Elliot Rosen (IU School of Medicine), Dr. Bruce D. Ray (Dept. of Physics, IUPUI), Dr. Sergio Funari (Deutsches Elektronen-Synchrotron), Dr. Mangilal Agarwal (INDI Center, IUPUI), Ryan Lybarger, Andrew K. Fraser, Lucas Burke, Taylor Segally, and Jason Kim for their advice, collaboration, support, insightful discussions and for sharing resources.

A portion of this research was performed on the EQ-SANS instrument at ORNL's Spallation Neutron Source and was sponsored by the Scientific User Facilities Division, Office of Basic Energy Sciences, U.S. Department of Energy (DOE).

A portion of this research was performed at the Chemical and Materials Science X-ray Science Division, Beamline 12ID-C, Advanced Photon Source. Use of the Advanced Photon Source, an Office of Science User Facility operated for the U.S. DOE Office of Science by Argonne National Laboratory, was supported by the U.S. DOE under Contract No. DE-AC02-06CH11357.

A portion of this research was performed at the Integrated Nanosystems Development Institute, IUPUI.

TABLE OF CONTENTS

	Page
LIST OF TABLES	vii
LIST OF FIGURES	viii
SYMBOLS	xi
ABBREVIATIONS	xii
ABSTRACT	xiv
1 INTRODUCTION	1
1.1 Chemical specificity versus material properties	1
1.2 Proteins	3
1.3 Protein nanomaterials	4
2 THEORY	8
2.1 Small-angle Scattering	8
2.2 Radius of gyration	9
2.3 Guinier Approximation	9
2.4 Pair Distribution Function	10
3 MATERIALS AND METHODS	11
3.1 Materials	11
3.1.1 A1AT Samples	11
3.1.2 Fibrinogen Samples	12
3.1.3 Lipid samples	12
3.2 Experimental Methods	12
3.2.1 Small-angle X-ray Scattering	12
3.2.2 Small-angle Neutron Scattering	13
3.2.3 Dynamic Light Scattering	13
3.3 Data Analysis and Controls	13

	Page
3.3.1 Data analysis	13
3.4 Lipid scattering	16
3.5 Optimization and controls	17
4 RESULTS	25
4.1 Scattering measurements of A1AT in solution	25
4.2 A1AT under osmotic pressure	31
4.3 A1AT and lipid	37
4.4 Fibrin polymerization	43
4.5 Fibrinogen under osmotic pressure	47
5 DISCUSSION	50
6 CONCLUSIONS	56
REFERENCES	57
VITA	66

LIST OF TABLES

Table	Page
3.1 Scattering length matching for contrast measurements.	23

LIST OF FIGURES

Figure	Page
1.1 Crystal structure of alpha-1-antitrypsin in two types of representations: cartoon view (top) and spacefill view (bottom). PDB structure 2QUG. DOI: 10.2210/pdb2QUG/pdb.	4
1.2 Crystal structure of fibrinogen in two types of representations: cartoon view (top) and spacefill view (bottom). PDB structure 3GHG. DOI: 10.2210/pdb3GHG/pdb	5
2.1 Schematics of small angle scattering setup.	8
3.1 SAXS 2D frame collected from the Argonne APS instrument and reduced to a 1D scattering curve.	15
3.2 Example of a Guinier fit, for SANS A1AT in 100% D ₂ O sample, using Igor Pro 6.0.	16
3.3 Examples of loaded fibrinogen (4.78 mg/ml) with thrombin (in concentrations of 0.005, 0.01, 0.03, 0.5 and 2.0 unit/ml; from left to right) samples into the banjo (quartz) holders for SANS measurements.	17
3.4 Examples of cloudy samples of fibrinogen (4.3 mg/ml) mixed with PEG 1500 (at 10 wt%, 20 wt%, and 30 wt%; from left to right) that show protein aggregation.	18
3.5 Example of a fibrinogen sample after polymerization; showing fibrin filaments.	19
3.6 Background measurements for SAXS.	20
3.7 Ellipsoid volume as a function of the Q_{max} cutoff from a model analysis using SasView for different samples. Q_{min} was kept constant at 0.01 \AA^{-1}	21
3.8 Plot of interpolated scattering intensity at $Q = 0$ for PEG 1500 solutions in mixtures as a function of D ₂ O fraction to determine matching scattering length density. The contrast match point is at the intersection of the data points with the line at 0 scattering intensity.	22
3.9 Radiation control of A1AT+POPC sample at 200 msec intervals. Upper panel shows the full measured Q range and the lower panel shows the scattering due to the POPC lipid.	24

Figure	Page
4.1 SAXS concentration series of A1AT in H ₂ O 1xPBS measured at 30°C. Lower panel shows the scattering curves with the background (capillary and H ₂ O 1xPBS) subtracted.	26
4.2 A plot of $I(0)$ versus A1AT concentration.	27
4.3 SANS of A1AT in D ₂ O 1xPBS. Experiments done at EQ-SANS beamline at ORNL-SNS.	28
4.4 SANS of A1AT in solution at different D ₂ O/H ₂ O ratios.	29
4.5 Patterson functions (pair distance distributions) for the A1AT concentration series obtained from SAXS.	30
4.6 SAXS Analysis of R_g using different models for the concentration series of A1AT samples.	31
4.7 Volume analysis of A1AT for three different shape models.	32
4.8 Calculated SANS curve for A1AT using the x-ray crystal structure (2QUG) and the program CRYSON.	33
4.9 SANS of A1AT in 50 wt% of PEG 1500.	34
4.10 SANS of pre-diluted A1AT under osmotic stress at 30°C.	34
4.11 Radius of gyration of A1AT as a function of PEG concentration as determined from SANS data using Igor Pro Guinier fit.	35
4.12 SAXS measurements of A1AT in PEG 1500 solutions (upper panel) and background scans (lower panel).	36
4.13 SAXS measurements of samples containing A1AT protein and POPC lipid vesicles in H ₂ O 1XPBS solution at 30°C. The upper panel shows the full measured range while the lower panel zooms on the 1st lipid peak.	38
4.14 SANS measurements of A1AT+POPC samples in 40% D ₂ O/H ₂ O mixture and of POPC alone in 40% D ₂ O/H ₂ O and in 100% D ₂ O	39
4.15 SAXS of POPS lipid and of POPS with A1AT.	40
4.16 SANS of POPS in solution, and POPS with A1AT while matching protein to the background to observe POPS.	41
4.17 SAXS measurements of samples containing A1AT protein and DLPC lipid vesicles in H ₂ O 1XPBS solution at 30°C. The upper panel shows the full measured range while the lower panel zooms on the 2nd lipid peak.	42

Figure	Page
4.18 SANS of fibrin polymerization using 5 mg/ml fibrinogen and 1 μ l of Thrombin (1 unit/ μ l), in 80% D ₂ O solvent). Each profile is accumulated over 5 minute time windows starting at the timepoints indicated by the labels.	44
4.19 Average size (diameter) of fibrin particles measured by DLS as a function of time. Different curves correspond to different amounts of fibrinogen (Fg) and thrombin (Thr) enzyme in the sample.	45
4.20 SANS of fibrin polymerization using 4.25 mg/ml fibrinogen and 0.01 μ l of Thrombin (1 unit/ μ l), in 80% D ₂ O solvent). Each profile is accumulated over various time intervals as shown on the legend.	46
4.21 PDF of Fibrin Formation Kinetics obtain from a GNOM analysis.	46
4.22 SANS profiles for fibrinogen in water and in 40% PEG 1500.	47
4.23 Analysis of fibrinogen under osmotic stress using GNOM for a rod-like model (upper panel) and a sphere-like model (lower panel).	48
5.1 Radius of gyration of A1AT as a function of PEG concentration as determined from SANS data using Igor Pro Guinier fit. The figure shows a linear fit to the compression regime at low osmotic pressure and the shading indicates protein aggregation.	52

SYMBOLS

b_D	Neutron scattering length of deuterium
b_H	Neutron scattering length of hydrogen (proton)
D_2O	Heavy water
$I(0)$	Scattered intensity at zero angle
$P(r)$	Pair distribution function
q, Q	Scattering vector
R_g	Radius of gyration
$wt\%$	Weight percentage
λ	Wavelength

ABBREVIATIONS

12-ID-C	Beamline at Argonne National Laboratory
2QUG	Crystal structure of alpha-1-antitrypsin
3GHG	Crystal structure of human fibrinogen
A1AT	Alpha1-antitrypsin proteinase inhibitor
AFM	Atomic force microscopy
APS	Advanced Photon Source
Arb	Arbitrary Units
A.U.	Arbitrary Units
BL6	Beamline 6 at SNS in Oak Ridge National Laboratory
DLPC	1,2-Dilauroyl-sn-glycero-3-phosphorylcholine
DLS	Dynamic light scattering
EQ	Extended Q-range
ER	Endoplasmatic reticulum
Fg	Fibrinogen
GNOM	An indirect transform program for small-angle scattering data processing.
kDa	kiloDaltons (molecular weight)
MW	Molecular weight
ORNL	Oak Ridge National Laboratory
PBS	Phosphate buffered saline
PDB	Protein Data Bank (rscb.org)
PEG	Polyethylene glycol
PC	Phosphatidylcholine
POPC	1-palmitoyl-2-oleoyl-sn-glycero-3-phosphocholine

POPS	1-palmitoyl-2-oleoyl-sn-glycero-3-phospho-L-serine
PS	Phosphatidylserine
SAS	Small-angle scattering
SAXS	Small-angle x-ray scattering
SANS	Small-angle neutron scattering
SNS	Spallation Neutron Source
Thr	Thrombin

ABSTRACT

Palacio, Luis A. Ph.D., Purdue University, May 2020. SMALL ANGLE SCATTERING OF LARGE PROTEIN UNITS UNDER OSMOTIC STRESS. Major Professor: Horia I. Petrache.

Large protein molecules are abundant in biological cells but are very difficult to study in physiological conditions due to molecular disorder. For large proteins, most structural information is obtained in crystalline states which can be achieved in certain conditions at very low temperature. X-ray and neutron crystallography methods can then be used for determination of crystalline structures at atomic level. However, in solution at room or physiological temperatures such highly resolved descriptions cannot be obtained except in very few cases. Scattering methods that can be used to study this type of structures at room temperature include small-angle x-ray and neutron scattering. These methods are used here to study two distinct proteins that are both classified as glycoproteins, which are a large class of proteins with diverse biological functions. In this study, two specific plasma glycoproteins were used: Fibrinogen (340 kDa) and Alpha 1-Antitrypsin or A1AT (52 kDa). These proteins have been chosen based on the fact that they have a propensity to form very large molecular aggregates due to their tendency to polymerize. One goal of this project is to show that for such complex structures, a combination of scattering methods that include SAXS, SANS, and DLS can address important structural and interaction questions despite the fact that atomic resolution cannot be obtained as in crystallography. A1AT protein has been shown to have protective roles of lung cells against emphysema, while fibrinogen is a major factor in the blood clotting process. A systematic approach to study these proteins interactions with lipid membranes and other proteins, using contrast-matching small-angle neutron scattering (SANS), small

angle x-ray scattering (SAXS) and dynamic light scattering (DLS), is presented here. A series of structural reference points for each protein in solution were determined by performing measurements under osmotic stress controlled by the addition of polyethylene glycol-1,500 MW (PEG 1500) in the samples. Osmotic pressure changes the free energy of the molecular mixture and has consequences on the structure and the interaction of molecular aggregates. In particular, the measured radius of gyration (R_g) for A1AT shows a sharp structural transition when the concentration of PEG 1500 is between 33 wt% and 36 wt%. Similarly, a significant structural change was observed for fibrinogen when the concentration of PEG 1500 was above 40 wt%. This analysis is applied to a study of A1AT interacting with lipid membranes and to a study of fibrinogen polymerization in the presence of the enzyme thrombin, which catalyzes the formation of blood clots. The experimental approach presented here and the applications to specific questions show that an appropriate combination of scattering methods can produce useful information on the behavior and the interactions of large protein systems in physiological conditions despite the lower resolution compared to crystallography.

1. INTRODUCTION

Scattering methods that include x-ray, neutron, and visible light scattering are a class of experimental physical methods used to obtain information on the structure of materials that are either in solid or liquid crystalline (gel) states. Biological materials that are made primarily of amino acids (proteins), fatty acids (lipids), and nucleotides (DNA) are classified as gel-like/colloidal/liquid-crystalline materials that exhibit a significant degree of molecular disorder in aqueous solutions at room temperature. Because of molecular disorder, while scattering measurements are often straightforward, data analysis is very complex involving extensive numerical analysis and a number of assumptions.

X-ray scattering is a method that is used primarily to investigate order structures such as crystals [1]. However, it can also be used to characterize less organized materials by providing information on granularity, inhomogeneities, and in general by providing a histogram of pairwise distances in the scatterer. Protein crystallography [2, 3] relies on finding conditions in which proteins arrange themselves in organized structures amenable to conventional x-ray [1, 4] or neutron scattering. In crystallography, one collects scattered intensities over a wide range of angles that correspond to lattice spacings from about 10 \AA (typical of amino acid sizes) down to 1 \AA corresponding to atomic size. In contrast, in small-angle scattering [5–8], the relevant scattering domain corresponds to much larger distances on the order of 10^2 \AA corresponding to the size of protein domains comprising many amino acid units.

1.1 Chemical specificity versus material properties

In studying biological molecules one faces two complementary aspects. On one hand, chemical compounds present in biological cells undergo chemical modifications

over various timescales as a result of enzymatic reactions and other chemical reactions. On the other hand, biological materials also exhibit physical properties that determine the structural integrity as well as the softness and adaptability required for proper biological function [9–11]. Lipid molecules, for example, are structural components of cell boundaries (*i.e.* membranes) and at the same time also act as substrates for a variety of enzymatic reactions such as the action of phospholipases, as well as acting as targets for a large array of cellular signaling events [12]. Being relatively small, (phospho)lipids can act as structural components only collectively by aggregating together [13]. Individual lipids as such do not have intrinsic structural roles – their large-number aggregates do.

The situation is more nuanced in the case of proteins. Many types of proteins are large sequences of hundreds and thousands of amino acids and their structural role is self-evident on the virtue of their sheer size, as for example in the case of collagen [14–17] and of actin [18–20] which are protein materials formed by polymerization. Amyloid fibrils [21–29] are another example of protein aggregates with macromolecular size. In essence, one can identify a structural role of proteins and especially protein aggregates simply based on their large physical size. At the same time, most known proteins are also participants in chemical reactions and/or molecular binding events that are the basis of the so called “molecular recognition” or cell signaling in biological systems. In such cases, proteins have been shown to have an “active site” where this molecular recognition occurs. Typically, these active sites are structurally small compared to the protein itself. One interesting question therefore is why chemically active proteins are physically so much larger than the chemically active site. Intuitively, the large size of the protein has the role to protect the active site either from chemical degradation or physical perturbation. In support of this interpretation, proteins have been shown to undergo significant structural changes which can turn on or off the active site. Although the exact way in which the sheer size of a protein “protects” its active site is not known, we work with the hypothesis that the properties of the protein material must play an important role. By regard-

ing the protein as a material rather than a particular chemical structure we focus on non-specific material properties rather than chemical specificity.

1.2 Proteins

Proteins are macromolecules that can assume a variety of conformations depending on environmental conditions such as pH, ionic strength (salt content), and temperature. Proteins have essential biological functions related not only to their chemical structure but also to their physical properties. A first level of classification distinguishes between water soluble and water insoluble proteins, called hydrophilic and hydrophobic, respectively. At a finer detail, any given protein can contain hydrophilic and hydrophobic domains. The interaction between these domains determines how a protein behaves in the aqueous environment of cells [12, 23, 30–32]. At the next level of classification, from a physical perspective, there are proteins that exist in monomeric form (single units) and proteins that have aggregation tendencies to form dimers, trimers, and even larger polymeric units. The ability and tendency of proteins to aggregate and in some cases to form polymers has important consequences on how they perform biological functions [2, 33–37]. However, there is no general rule: the aggregation of some proteins is beneficial to cells while the aggregation of others is detrimental. In this project, we consider two representatives of proteins that are prone to aggregation and polymerization: alpha-1 antitrypsin (A1AT) and fibrinogen.

A1AT (Fig. 1.1), with a molecular weight of 52kDa (400 amino acids) is a member of a protein family called serpins [30, 38–48]. It has been shown to have protective roles of lung cells against emphysema, a disease characterized by lung tissue destruction. [49–51]. Fibrinogen (Fig. 1.2), with a molecular weight 340 kDa (3000 amino acids) is the building block of blood clots [42, 45, 52–57]. While biologically distinct, the two proteins present similarities in biophysical studies due to their large size and their aggregation and polymerization tendencies.

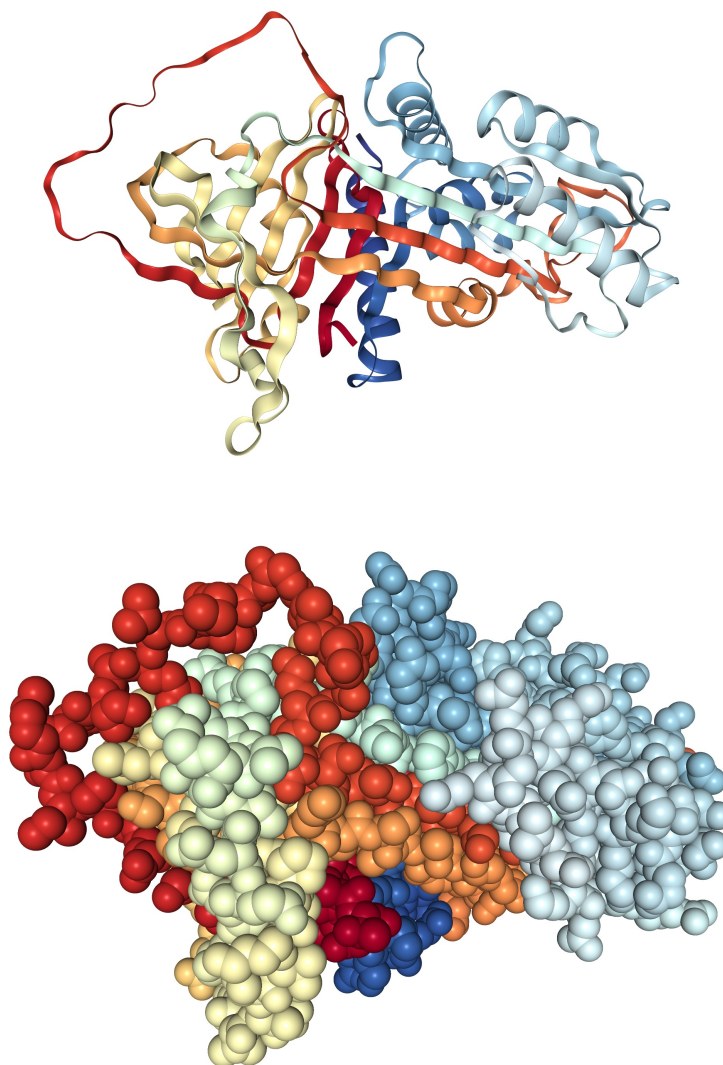


Fig. 1.1. Crystal structure of alpha-1-antitrypsin in two types of representations: cartoon view (top) and spacefill view (bottom). PDB structure 2QUG. DOI: 10.2210/pdb2QUG/pdb.

1.3 Protein nanomaterials

Although inspired from biology, the main focus in this thesis is on the material properties of protein structure and aggregates. This material perspective is a con-

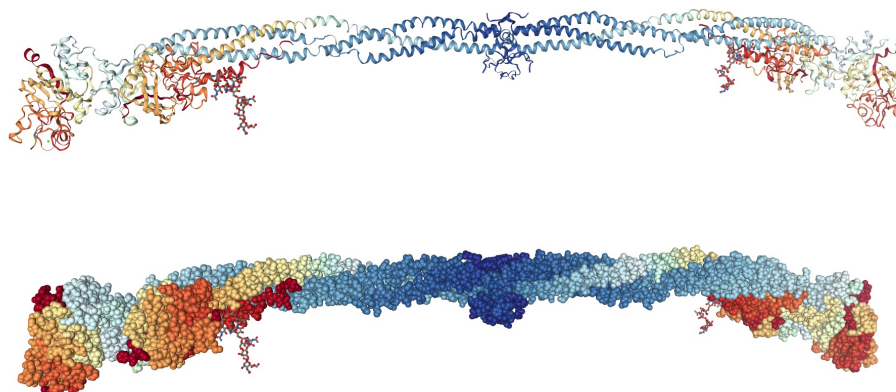


Fig. 1.2. Crystal structure of fibrinogen in two types of representations: cartoon view (top) and spacefill view (bottom). PDB structure 3GHG. DOI: 10.2210/pdb3GHG/pdb

sequence of current interest in industry and technology in nanomaterials [9–11, 14, 58–64]. The bioinspired branch of material engineering takes advantage of molecular constructs that (1) already exist in nature, (2) can be readily produced at large scales and (3) have tunable material properties. Networks of polymerized or simply aggregated proteins are excellent candidates for uncovering natural products for new applications.

A number of physical methods are available to study and characterize soft, gel-like materials. These include scattering methods such as x-ray, neutron, and visible as well as force spectroscopy such as AFM. In this thesis, we use small-angle scattering methods which are appropriate for scatterers that are much larger than the wavelength of the radiation used in the measurement. As a reference, typical x-ray and neutron wavelengths used in material research are on the order of 1 – 10 Å, while protein aggregates have sizes that range from nanometers to microns. While small-angle x-ray scattering (SAXS) and small-angle neutron scattering (SANS) are by now established methods [3, 8, 35, 65–72], the challenging aspect of this thesis is the heterogeneity

and polydispersity of protein samples prone to aggregation and polymerization. In other words, acquiring and analyzing scattering data involve considerations of sample preparation history and polymerization conditions. In the case of fibrinogen, it is well known from physiological and molecular studies that it polymerizes in the presence of an enzyme called thrombin forming a network aggregate call fibrin, essentially the blood clot. For A1AT, polymerization seems to occur spontaneously in certain conditions although there is no clear conclusion at this point. Misfolding and aggregation of A1AT has been reported in a cell organelle called endoplasmatic reticulum (ER). [51, 73] Some misfolding is concurrent with polymerization which then leads to "ER overload", which is basically mechanical stress. Mutations in the amino acid sequence of the protein might be responsible for this process.

The primary data for this project are small-angle x-ray scattering (SAXS) measurements performed at the Advanced Photon Source (APS) at the Argonne National Laboratory (ANL) and small-angle neutron scattering measurements (SANS) at the Oak Ridge National Laboratory (ORNL). The EQ-SANS (BL6) instrument at ORNL was used for SANS experiments [69], while SAXS data were collected at the X-ray Operations and Research Beamline 12-ID-C at the APS. SAXS and SANS [71] are complementary methods and each instrument has its own advantages and disadvantages. Most notably, the intensity of a synchrotron beam is much higher than that of a neutron source. This translates into short exposure times for SAXS experiments (order of milliseconds), and long exposure times for SANS experiments (order of hours). There are a few important advantages of SANS over SAXS: SANS does not result on radiation damage of the sample, while SAXS does; SANS is sensitive to hydrogen and to isotopes, while SAXS is not; and the penetration depth of neutrons is higher than that of x-rays. Neutrons interact with the nuclei, the electron shell and in an unsystematic way with the atomic number, depending on the direction of the nuclear spin. X-rays interact with the electron shell and the interaction is proportional to the atomic number of atoms. Hydrogen is virtually invisible to x-rays.

Structural measurements in this project are performed for samples under osmotic stress which is controlled by the addition of polyethylene glycol polymer (PEG). PEG has been shown to have negligible specific interactions with biological molecules including lipids, protein, and DNA, while acting as an effective osmolyte. Such an approach is therefore appropriate for our goal here to study the non-specific material properties of protein aggregates as opposed to chemical specificity.

2. THEORY

2.1 Small-angle Scattering

In this work we are only concerned with elastic scattering. This means that there is no change in the wavelength λ and no change in momentum magnitude $k_s = k_i$. However, the direction (orientation) of the momentum vector of the beam upon interacting with the sample changes as

$$|\vec{q}| = |\vec{k}_s - \vec{k}_i| = \frac{4\pi \sin(\theta)}{\lambda}, \quad (2.1)$$

where 2θ is the scattering angle. Figure 2.1 shows a schematic of scattering geometry.

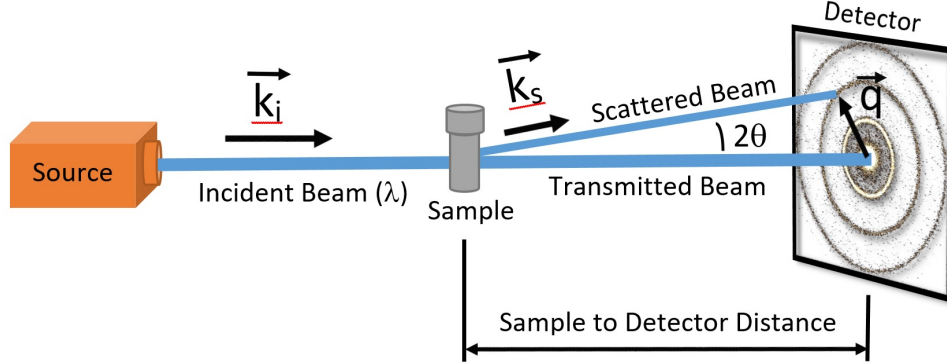


Fig. 2.1. Schematics of small angle scattering setup.

The intensity of the scattered beam is given by

$$I(q) = \left\langle \left| \int (\rho(\vec{r}) - \bar{\rho}_s) e^{i\vec{q}\cdot\vec{r}} d\vec{r} \right|^2 \right\rangle, \quad (2.2)$$

where $\rho(\vec{r})$ is the scattering length distribution (equal to the total scattering length of the atoms per unit volume) and $\rho(\vec{r}) - \bar{\rho}_s$ is the difference in scattering density

between the volume element at position \vec{r} and that of the solvent. The difference is called the scattering contrast

$$\Delta\rho = \rho(\vec{r}) - \bar{\rho}_s. \quad (2.3)$$

2.2 Radius of gyration

One convenient parameter used to measure the size of a solid object is its radius of gyration which is defined as

$$R_g^2 = \frac{1}{2} \frac{\int_0^\infty r^2 p(r) dr}{\int_0^\infty p(r) dr} \quad (2.4)$$

where $p(r)$ is the length distribution function of the object. Note that this is not the same as the physical boundary of the object. For example, for a solid and uniform triaxial ellipsoid of semiaxes a , b , and c the square of the radius of gyration is

$$R_g^2 = \frac{1}{5}(a^2 + b^2 + c^2). \quad (2.5)$$

For a sphere we have $a = b = c = R$ and the formula reduces to

$$R_g^2 = \frac{3}{5}R^2. \quad (2.6)$$

For a solid and uniform cylinder of radius r and length L , the square of the radius of gyration is

$$R_g^2 = \frac{1}{12}(3r^2 + 4L^2). \quad (2.7)$$

These models are implemented in the Igor software used for fitting scattering data.

2.3 Guinier Approximation

The Guinier approximation is the results of truncating a power series expansion which for globular molecules gives

$$I(q) = I(0) e^{-\frac{q^2 R_g^2}{3}} \quad (2.8)$$

and which, in theory, is valid when

$$\frac{q^2 R_g^2}{3} < 1. \quad (2.9)$$

In practice, a safer limit of $q_{max} R_g < 1.3$ or even $q_{max} R_g < 1$ is considered when scattering data are analyzed in this way. Where q_{max} is the maximum q value on the range being considered for the Guinier fit. By taking the log of Eq. 2.8, we obtain

$$\ln [I(q)] = \ln [I(0)] - \frac{q^2 R_g^2}{3}. \quad (2.10)$$

The Guinier approximation can be used to estimate the forward scattering $I(0)$ by extrapolation to low q and to obtain the radius of gyration R_g from the slope of the $\ln [I(q)]$ vs. q^2 plot.

2.4 Pair Distribution Function

A pair distribution function $P(r)$ of inter-atomic distances can be obtained by performing a Fourier transform of the scattering profile. Essentially, $P(r)$ is a histogram of distances between all pairs of atoms in the scatterer and can be used to detect changes in protein structure in real space. Boundary conditions are $P(0) = 0$ and $P(D_{max}) = 0$, where D_{max} is the upper limit for r and is usually estimated as $D_{max} \approx 3R_g$. The zeroth moment of $P(r)$ is the value $I(0)$,

$$I(0) = 4\pi \int_0^{D_{max}} P(r) dr, \quad (2.11)$$

while the second moment is related to the radius of gyration as given above in Eq. 2.4. The value $I(0)$ is proportional to the number of scattering particles N per unit volume and the volume of the particle V ,

$$I(0) = N(\Delta\rho V)^2 = \frac{C(\Delta\rho)^2 v^2 M_W}{N_A}, \quad (2.12)$$

where M_W is the molecular weight of the scattering particle, C is mass density, v is the partial specific volume of the particle, N_A is Avogadro's number, and $\Delta\rho$ is the density contrast.

3. MATERIALS AND METHODS

3.1 Materials

A1AT (alpha1-proteinase inhibitor (human)) was purchased in purified powder form from Baxter (Aralast). Phosphate Buffered Saline (PBS), 10X Solution, was purchased from Fisher BioReagents. Fibrinogen and Thrombin were provided by Dr. Elliott Rosen from the School of Medicine at Indiana University. PEG 1500 and PEG 400 (Poly-ethylene glycol average MW 1,500 and 400 respectively) were purchased from Sigma-Aldrich in solid form. The lipids POPC (1-Palmitoyl-2-oleoylphosphatidylcholine), POPS (1-palmitoyl-2-oleoyl-sn-glycero-3-phospho-L-serine) and DLPC (1,2-Dilauroyl-sn-glycero-3-phosphocholine) were purchased in purified powder form, and in chloroform solution from Avanti Polar Lipids. A1AT was stored at 4°C and fibrinogen at -80°C. Lipids were stored at -20°C for long terms (longer than 1-2 months) and at 4°C for shorter periods. PEG was stored at room temperature.

3.1.1 A1AT Samples

A1AT samples were prepared by directly diluting the protein powder into prepared buffer. For solutions containing A1AT and PEG, each solute was first dissolved at high concentrations to make stock solutions and then later diluted and combined to reach desired concentrations. 1X PBS (pH 7.4) was used for all samples that contained proteins. Vortexing was used to mix samples. Some samples required cycles of centrifugation and vortexing in order to create homogeneous mixtures. A series of 4 mg/ml A1AT samples (at 40% D₂O, to observe the PEG molecules) was made by varying the concentration of PEG 1500 from 0 wt% to 50 wt%. All A1AT measurements were done at 30°C.

3.1.2 Fibrinogen Samples

Because of the high propensity of fibrinogen to polymerization, even in the absence of thrombin, these samples required to be kept at the lowest possible temperature when not stored at -80°C . Dry ice was used to keep the samples frozen during transportation and before experiments were conducted. Transportation time to Oak Ridge National Laboratory was approximately 6 hours, and transportation time to Argonne National Laboratory was approximately 4 hours. Aliquots of fibrinogen and thrombin were thawed and allowed to equilibrate for at least 30 minutes before measurements, by placing them in a 30°C bath.

3.1.3 Lipid samples

Lipids in chloroform were lyophilized over an 8 hour period to obtain a lipid powder; which was then added to buffer solutions. Lipid dispersions were then vortexed and put through freeze/thaw cycles to obtain a homogeneous distribution of lipid vesicles [74]. Protein-lipid membrane samples were prepared by mixing (nominal concentrations) 4 mg/ml A1AT and 10 mg/ml lipid in 1X PBS solution. Mixtures were then vortexed/centrifuged and stored at 4°C . Before measurements, samples were equilibrated at measurement temperature, and vortexed to obtain a homogeneous sample that was added to capillaries (SAXS) and banjos (SANS) for measurement.

3.2 Experimental Methods

3.2.1 Small-angle X-ray Scattering

SAXS measurements were performed at the X-ray Operations and Research Beamline 12-ID-C at the Advanced Photon Source, Argonne National Laboratory. All of the data were provided in frame (picture of the scattering) format, and as a 1-D reduced text file ready to be analyzed.

3.2.2 Small-angle Neutron Scattering

SANS measurements were performed at the EQ-SANS (BL6) instrument at Oak Ridge National Laboratory (ORNL) in Oak Ridge, TN; during five beam-times awarded under the Integrated Proposal Tracking System. These are IPTS-6362, IPTS-7367, IPTS-8479, IPTS-9237, and IPTS-10118. All of the raw data was archived by the U.S. Department of Energy under each beam-time IPTS number. Raw data files were then reduced using Mantid software and the instrument parameters to produce the 1D text files that could be analyzed using Igor and SasView.

The EQ-SANS instrument has a detector on rails that allows for the sample to detector distance to be adjusted and has choppers that allow for the user to adjust the wavelength of the neutrons. Because of these adjustable parameters its Q range is $0.002 \text{ \AA}^{-1} - 1.4 \text{ \AA}^{-1}$. The detector size is 1m x 1m, and has 192 tubes x 256 divisions; for a detector resolution of 5.5mm x 4.3mm. This instrument offers a sample-to-detector distance range of 1.3m – 9m, and has a bandwidth of $3 \text{ \AA} - 4.3 \text{ \AA}$.

3.2.3 Dynamic Light Scattering

DLS measurements were done using a Malvern Zetasizer Nano ZS90 instrument available in the INDI Center at IUPUI.

3.3 Data Analysis and Controls

3.3.1 Data analysis

Most data analysis was performed using the software Igor and its free variant SasView together with data reduction packages provided by the Oak Ridge National Laboratory for SANS and the Argonne National Laboratory for SAXS. For both SAXS and SANS, analysis packages accounted for beamline geometry, beam wavelength, and detector resolution and sensitivity.

The 2D frame collected from the instrument is converted into a 1D scattering curve (Fig. 3.1) by integrating over the scattering arc. The Argonne APS SAXS instrument was set to collect data over 90 degrees. The purpose of using a quarter of the frame was to obtain data over a larger Q range. This is possible because the signal to noise ratio is usually strong enough that a full frame is not needed. The 1D curve is translated into a readable text file that can be used for analysis. The reduction process also involves input of instrument parameters and various calibration (i.e. empty cell, background, and transmission) files.

Guinier analysis of A1AT SAXS data: The SAS raw data were reduced from 2D detector data to 1D by integration. Before fitting the data, the constant background and buffer background were subtracted aligned at high Q ($0.3 \text{ \AA}^{-1} - 0.5 \text{ \AA}^{-1}$) and subtracted. In the case of SAXS the buffer background also included solutes that were not being subject to the investigation. Most of the small angle scattering (SAS) data fitting and analysis was done using SasView 4.01. The KCL SAS Analysis package of Igor Pro 6.01 was used for early experiments to perform Guinier analysis and to compare of raw data of scattering curves. Figure 3.2 shows how Igor Pro was used to extract R_g parameters from an A1AT concentration series. Fitting the data using Igor Pro is a manual iteration process that takes a very long time to complete compared to SasView, which has an automated process. Two types of data fittings were done: shape independent and shape dependent. The shape independent models were used to find radius of gyration (R_g) of the molecule being measured. The shape dependent models used are solid sphere, ellipsoid, and cylindrical ellipsoid for which fitting volumes were reported in order to compare between the different shapes.

Contrast matching: One of the advantages of using SANS to study a solution with two different type of molecules is that the solvent can be prepared in a manner where one of the molecule's scattering contribution blends with that of the solvent [53, 65, 67, 72, 75–77]. This in turn allows for the scattering contribution of the other molecule to be observed. This is possible due to the scattering length of hydrogen having an opposite sign (shift of π of the phase on scattering) to that of deuterium,

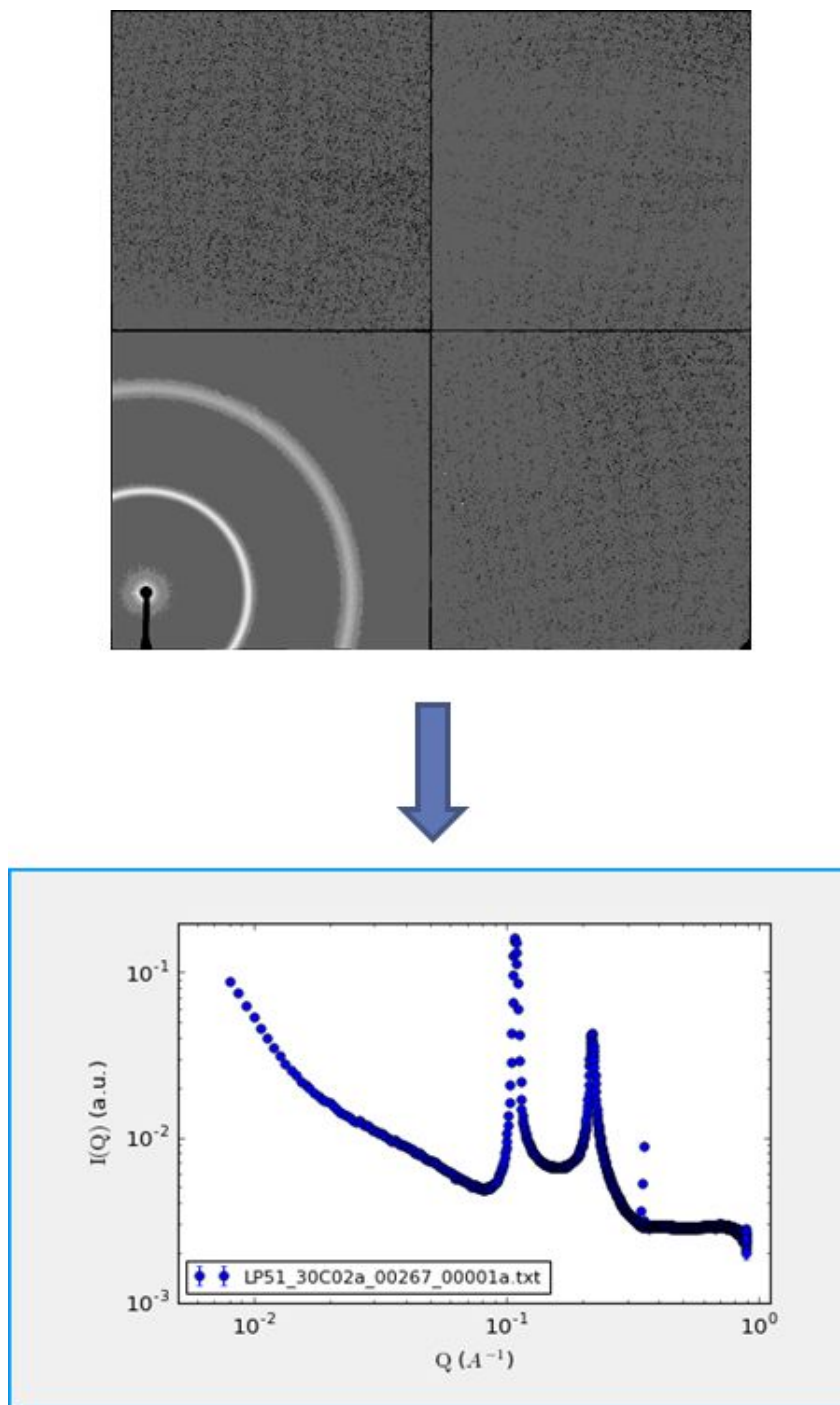


Fig. 3.1. SAXS 2D frame collected from the Argonne APS instrument and reduced to a 1D scattering curve.

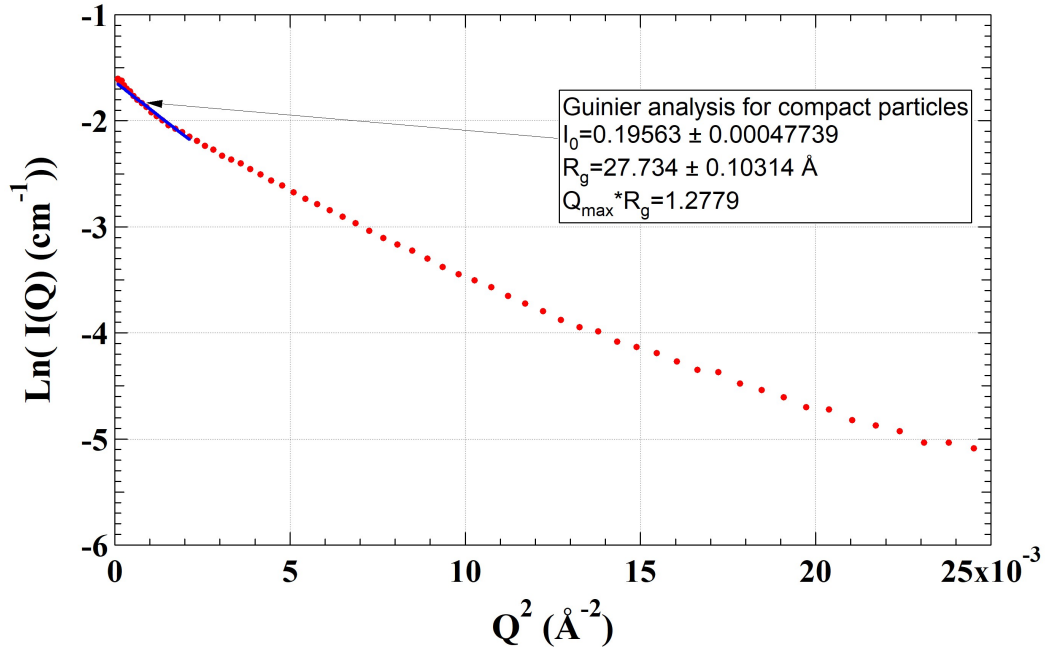


Fig. 3.2. Example of a Guinier fit, for SANS A1AT in 100% D₂O sample, using Igor Pro 6.0.

and a different magnitude: $b_H = -0.374 \cdot 10^{-12}$ cm and $b_D = 6.37 \cdot 10^{-12}$ cm. A prerequisite for the SANS osmotic stress experiments is to know the contrast match point for the molecules that are present in the solution.

3.4 Lipid scattering

Multilamellar lipid vesicles (MLVs) give rise to interference peaks at angles given by Bragg's law for a 1D lattice:

$$2D \sin \theta = h\lambda, \quad (3.1)$$

where D is the lattice spacing, θ is the angle of incidence, λ is the radiation wavelength, and h is an integer number. The lattice spacing D is the average distance between neighboring lipid membranes in the MLVs. The lipids used in this study



Fig. 3.3. Examples of loaded fibrinogen (4.78 mg/ml) with thrombin (in concentrations of 0.005, 0.01, 0.03, 0.5 and 2.0 unit/ml; from left to right) samples into the banjo (quartz) holders for SANS measurements.

are in a fluid state at room temperature and therefore give rise to no more than 2 interference peaks, therefore $h = 1, 2$.

3.5 Optimization and controls

Some of the key issues for analysis of scattering data are 1) background controls, 2) relevant Q -range for data analysis, 3) scattering length matching (contrast) for SANS, and 4) radiation damage.

1) Background controls. Fig. 3.6 shows one example of background measurements for SAXS in which different glass capillaries were measured while loaded with



Fig. 3.4. Examples of cloudy samples of fibrinogen (4.3 mg/ml) mixed with PEG 1500 (at 10 wt%, 20 wt%, and 30 wt%; from left to right) that show protein aggregation.

the same H_2O -1xPBS buffer solution. The exposure time for each sample was 0.2 sec which was typical for our measurements at APS. All measurements were done using Glass 50 capillaries, except otherwise specified.

The scattering profiles from glass capillaries loaded with buffer solution are clearly not flat and needed to be subtracted appropriately from the scattering data during data analysis. The functional form of the scattering curves is the same with and without the PBS buffer which simplifies data analysis to some extent. There are no major differences between the different types of capillaries except for different absorption coefficients which are approximately constant in the measured Q -range. Two of the scattering curves show “zingers” at high Q values which are sharp spikes due to either detector electronics, direct scattering in the detector, or cosmic radiation.



Fig. 3.5. Example of a fibrinogen sample after polymerization; showing fibrin filaments.

These zingers are detected and eliminated by data analysis packages and do not affect analysis results.

2) Relevant Q -range. As opposed to standard crystallography where scattering Bragg peaks are well defined, the analysis of SAXS profiles require testing the robustness of data analysis results with the selection of the Q -range to be analyzed. In principle, one aims to use the full range of scattering data, however there are a number of limitations that need to be considered: 1) data close to the beam center (low Q) are corrupted by overlap with the main beam and beam geometry, 2) data close to detector edges (usually high Q) are corrupted by detector construction, and 3) the analysis of both small-angle scattering (both SAXS and SANS) rely on struc-

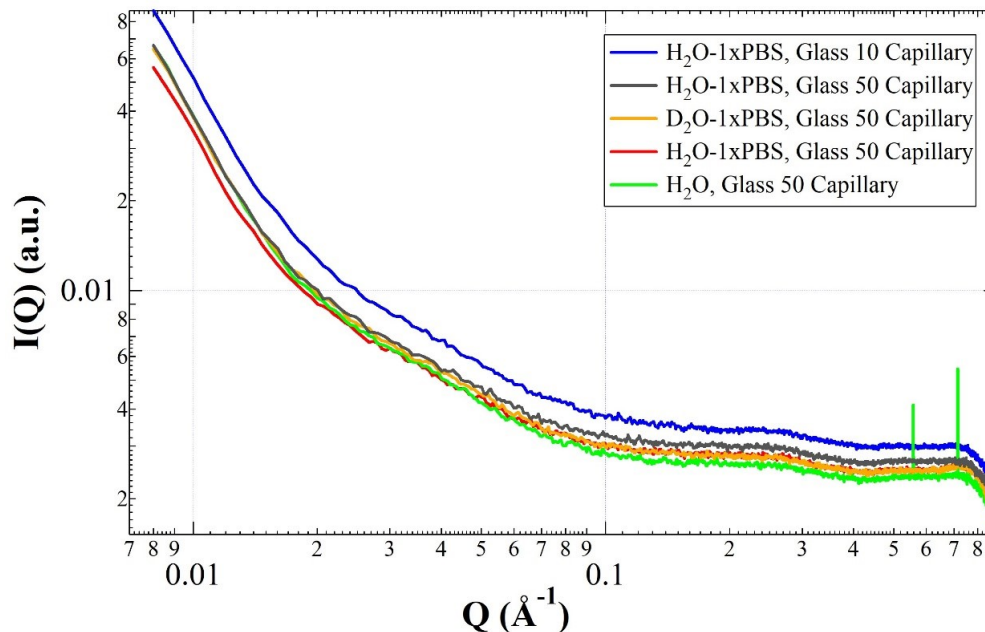


Fig. 3.6. Background measurements for SAXS.

tural models and approximations. Items 1) and 2) are for the most part taken into account by the analysis module available at each beamline. However, item 3) needs to be investigated for each system. Fig. 3.7 shows one example of such analysis in which an ellipsoid model was used to fit SAXS data. The plot shows the calculated ellipsoid volume as a function of the maximum Q cutoff. From scanning the Q_{max} for all samples in this concentration series it is clear that the upper limit of the Q range needs to be above 0.3 \AA^{-1} .

3) Scattering length matching. The contrast match point for lipids and proteins are known to be 15% and 40% v/v $\text{D}_2\text{O}/\text{H}_2\text{O}$ solvents, respectively (Madl et al., 2011, Parsegian et al., 2000) (Table 1). These are the $\text{D}_2\text{O}/\text{H}_2\text{O}$ v/v fraction that need to be avoided when trying to observe either molecule using SANS. Because the matching point of protein is near 40% $\text{D}_2\text{O}/\text{H}_2\text{O}$, it is important to accurately define the contrast match point for PEG 1500. A contrast match experiment was done using

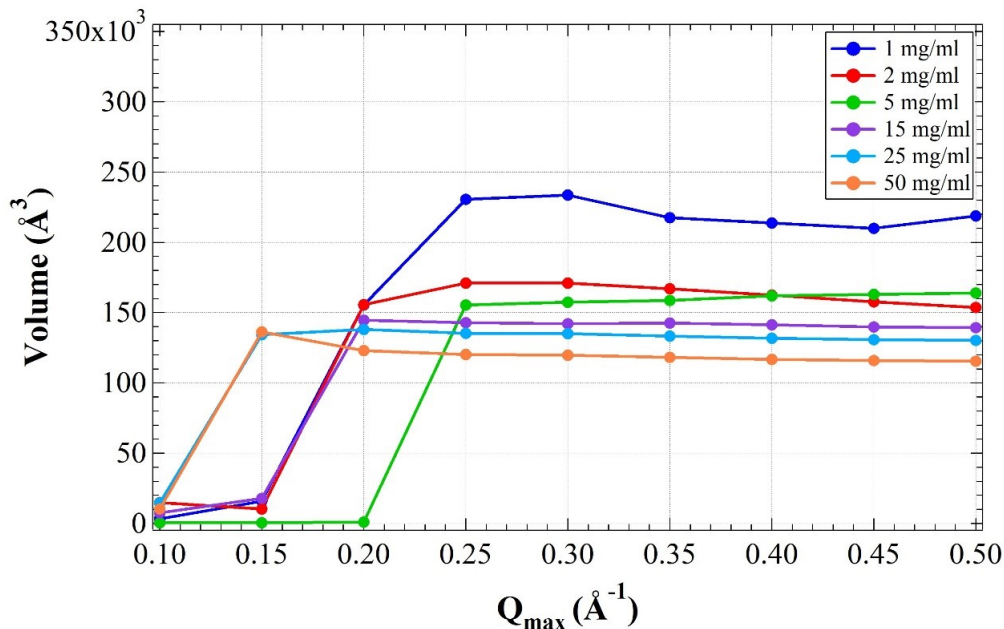


Fig. 3.7. Ellipsoid volume as a function of the Q_{max} cutoff from a model analysis using SasView for different samples. Q_{min} was kept constant at 0.01 \AA^{-1} .

10 wt% of PEG 1500 in solution and by varying the volume fraction of D_2O/H_2O of the solvent.

Figure 3.8 shows how the contrast match point for PEG 1500 was obtained. The figure shows a plot of interpolated scattering intensity at $Q = 0$ for PEG solutions in mixtures as a function of D_2O fraction. The set of measurements include three points under 20% and three points above 20% D_2O/H_2O solvent. The points were selected this way because the theoretical estimate placed the match point between 15% and 20%. The square root of the forward scattering intensity $I(0)$ is plotted versus the D_2O fraction of the solvent. Points below 20% D_2O were inverted so that a linear fit could be used to determine the match point of 16% D_2O/H_2O . The intersection of data points with the line at $I(0) = 0$ indicates the point of scattering matching between PEG 1500 and the D_2O/H_2O mixture (Contrast Match Point).

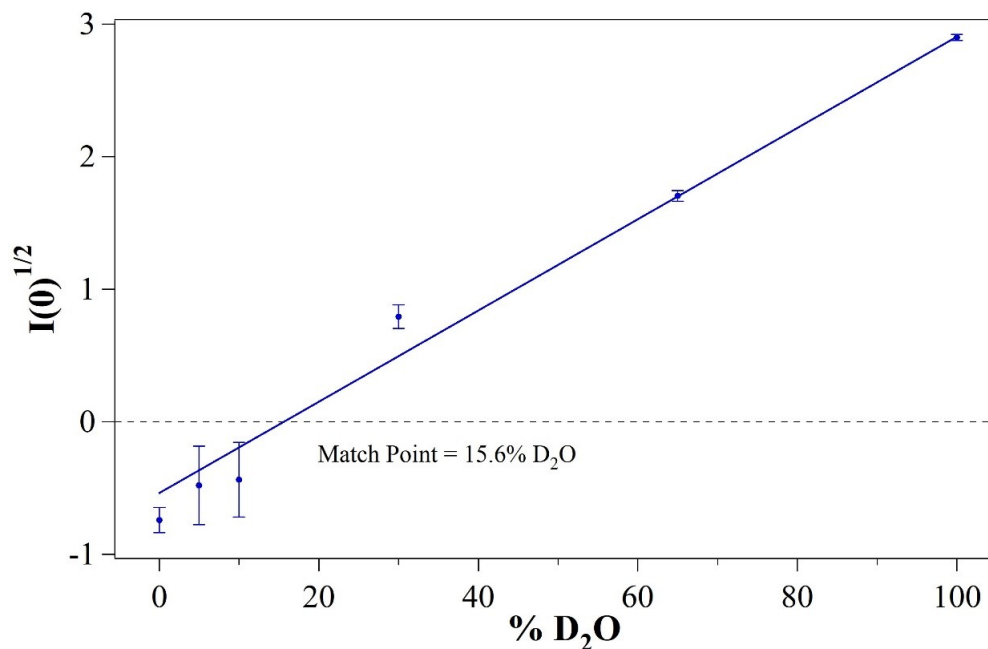


Fig. 3.8. Plot of interpolated scattering intensity at $Q = 0$ for PEG 1500 solutions in mixtures as a function of D₂O fraction to determine matching scattering length density. The contrast match point is at the intersection of the data points with the line at 0 scattering intensity.

Table 3.1 shows the D₂O/H₂O ratios that match the molecules of interest in this study, namely PEG 1500, protein, and lipid. While there are clearly differences in the scattering density for different proteins (as well as for different lipids) based on their chemical structures, these differences are negligible. Therefore current studies use generic protein and lipid matching scattering lengths.

4) Radiation damage. Fig. 3.9 shows an example of radiation damage testing for SAXS measurements of samples containing the A1AT protein and the POPC lipid. The upper panel shows the full measured range, while the lower panel shows a zoom on the lipid scattering portion. While there is no significant change in the lipid scattering, the range of Q values corresponding to protein scattering shows a systematic change versus time which is due to radiation damage. These control measurements were used to set the maximum scanning time per sample.

Table 3.1.
Scattering length matching for contrast measurements.

Molecule	$D_2O : H_2O$ ratio	Source
PEG 1500	16%	This work
Protein	40%	Madl et al., 2011
Lipid	15%	Parsegian et al., 2000

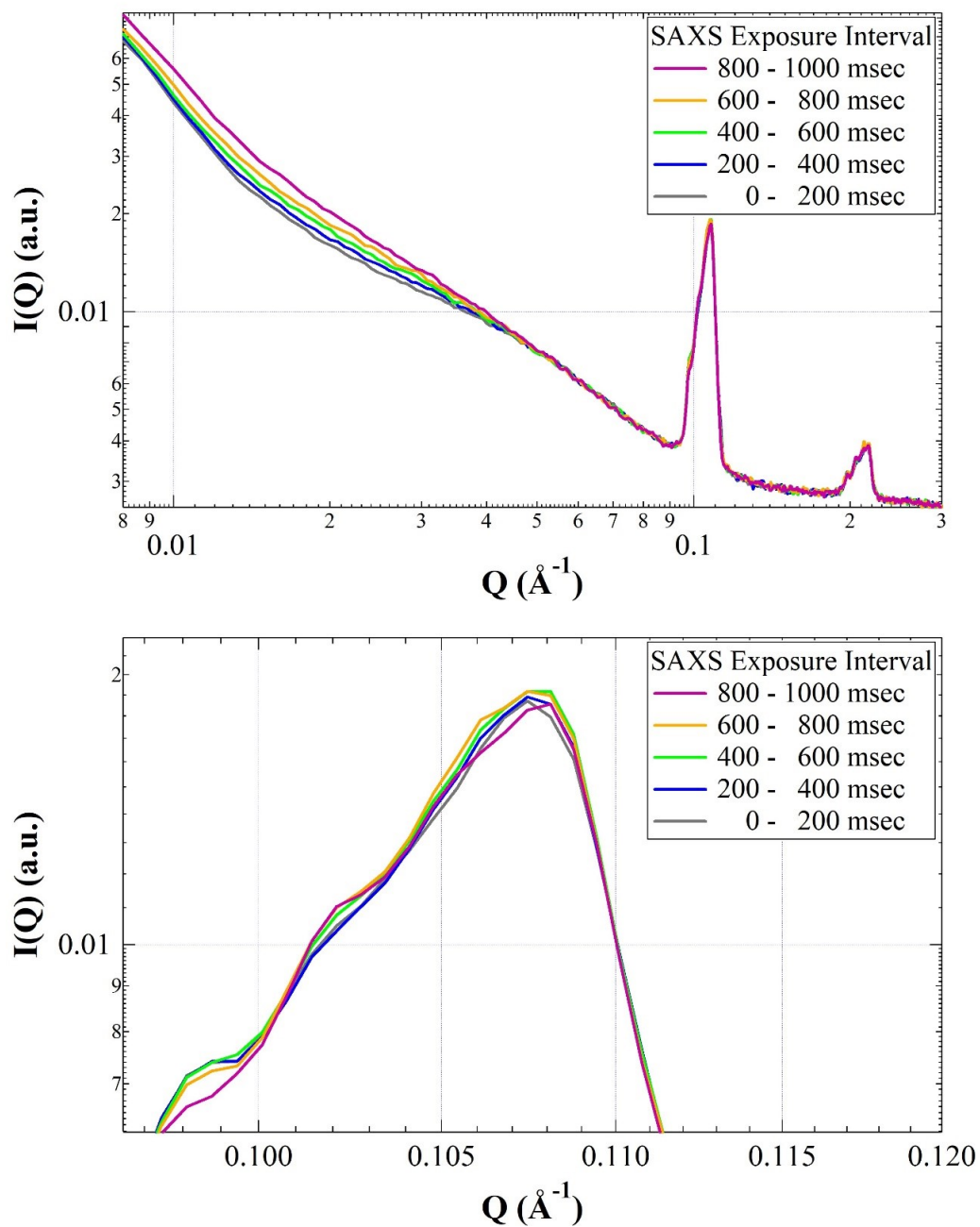


Fig. 3.9. Radiation control of A1AT+POPC sample at 200 msec intervals. Upper panel shows the full measured Q range and the lower panel shows the scattering due to the POPC lipid.

4. RESULTS

There are five sections of results as follows: 1) A1AT in solution, 2) A1AT under osmotic stress, 3) A1AT and lipid, 4) Fibrin polymerization, and 5) Fibrinogen under osmotic stress.

4.1 Scattering measurements of A1AT in solution

SAXS measurements of A1AT in H₂O (1xPBS buffer) at 30°C are shown in Fig. 4.1. The upper panel shows raw scattering curves that were processed only for beam geometry and detector sensitivity while the lower panel shows the scattering curves minus the background.

These samples were prepared within 30 hours of measurement in order to minimize the effect of A1AT polymerization tendency. Constant backgrounds were extrapolated from the range of Q values $0.3 \text{ \AA}^{-1} < Q < 0.4 \text{ \AA}^{-1}$ and the beam shape was subtracted for low Q . Measurements were done at beam line 12 ID-C using glass capillaries (1.5 - 2 mm path) with exposure times of 200 msec per scan. Beamline parameters were as follow: quantum energy was $h\omega = 18 \text{ KeV}$ corresponding to $\lambda = 0.6888 \text{ \AA}$, beam size is horizontally 0.5 mm and vertically 0.3 mm, the detector has 1024 by 1024 pixels, and the pixel size is 0.175 mm x 0.175 mm, and the sample detector distance is 2392 mm.

The figure shows that the scattering signal increases with increasing A1AT concentration as expected but the functional form does not change significantly as seen in the lower panel that shows background subtracted scans.

The intensity at $I(0)$ should linearly correlate to the concentration of the sample. Fig. 4.2 shows an χ^2 of 0.987. This graph was used to verify the concentration series

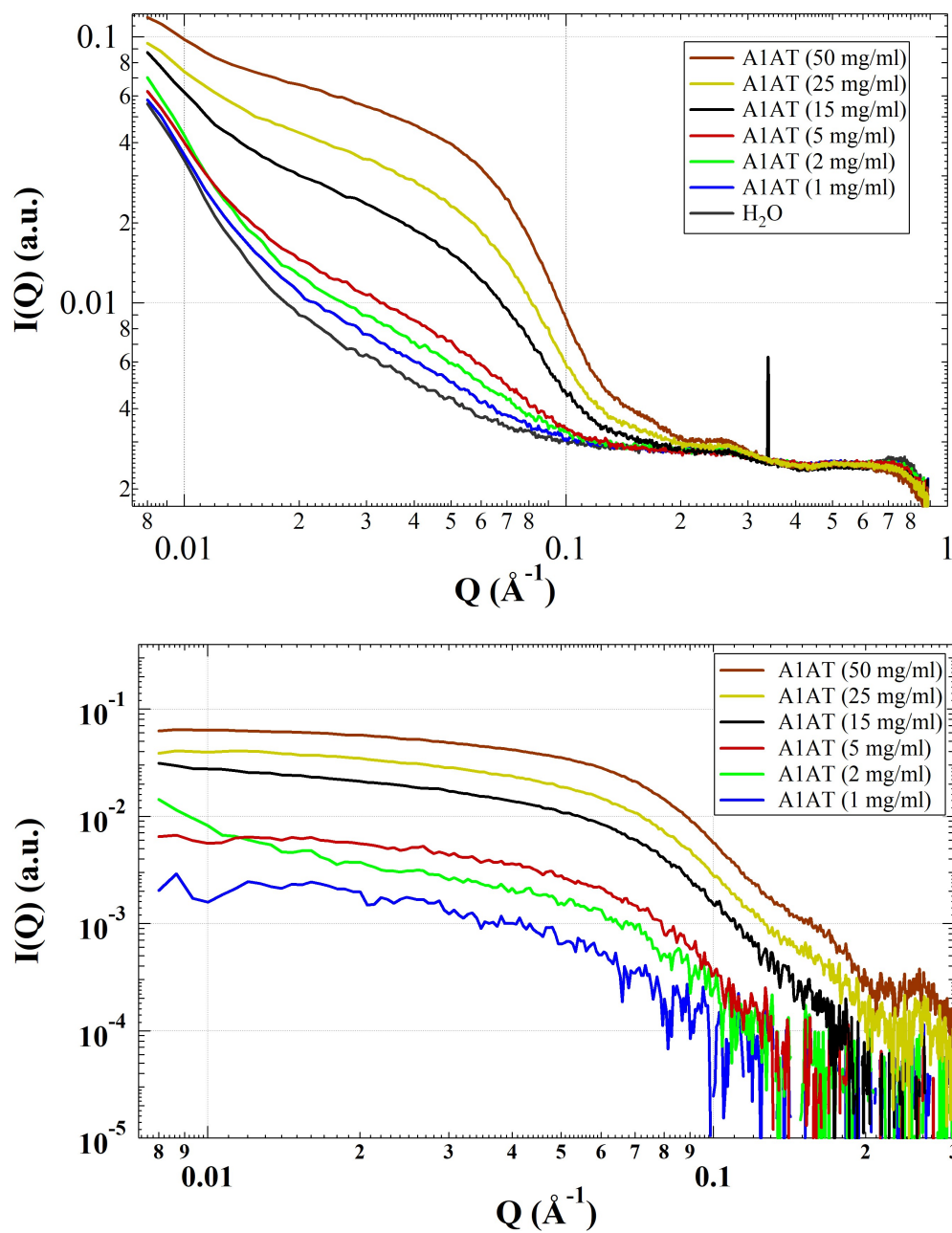


Fig. 4.1. SAXS concentration series of A1AT in H_2O 1xPBS measured at 30°C . Lower panel shows the scattering curves with the background (capillary and H_2O 1xPBS) subtracted.

of samples and to insure there are no significant experimental artifacts that might arise from both sample geometry and chemical composition.

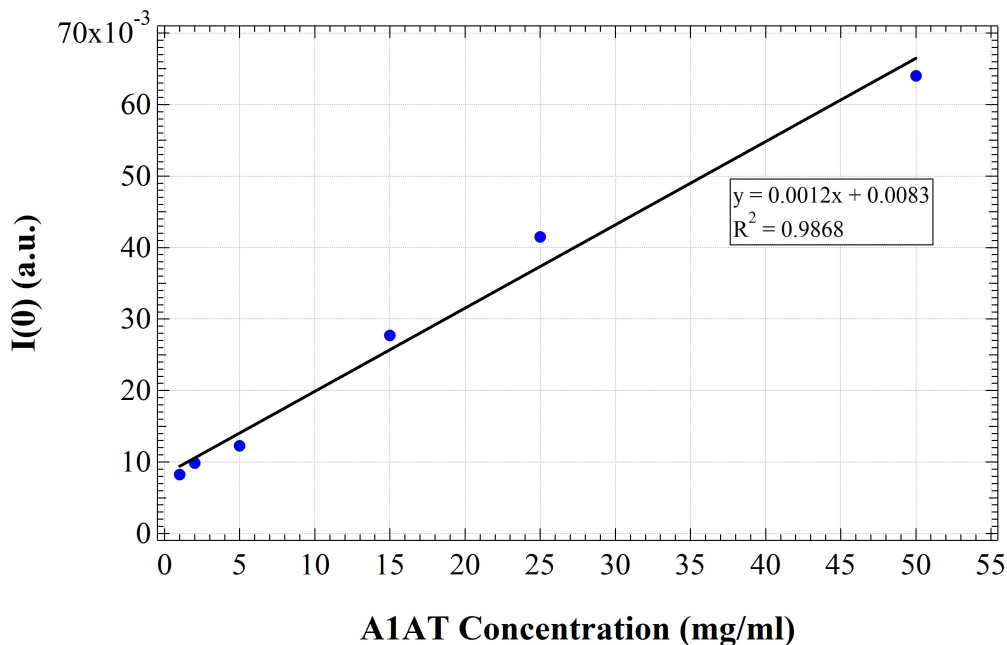


Fig. 4.2. A plot of $I(0)$ versus A1AT concentration.

Similar results are obtained from SANS measurements as shown in Fig. 4.3 which like before shows raw scattering curves in the upper panel and background subtracted curves in the lower pane. These experiments were done using a neutron wavelength of 2.5 \AA , and a sample to detector distance of 4 m. For background subtraction, the D_2O scattering was used as shown in the upper panel for the two types of sample holders (banjos) used in the experiment.

Fig. 4.4 shows SANS measurements of A1AT in solutions of different $\text{D}_2\text{O} / \text{H}_2\text{O}$ ratios used for scattering length contrast. The scattering was significantly weaker in 16% D_2O which is likely due to 16% D_2O being a closer to 40%, which is the match point for A1AT.

The Patterson functions of pairwise distances are shown in Fig. 4.5. The blue curve (2 mg/ml) represents the concentration in normal serum (i.e. 1.5 - 3.5 mg/ml). At

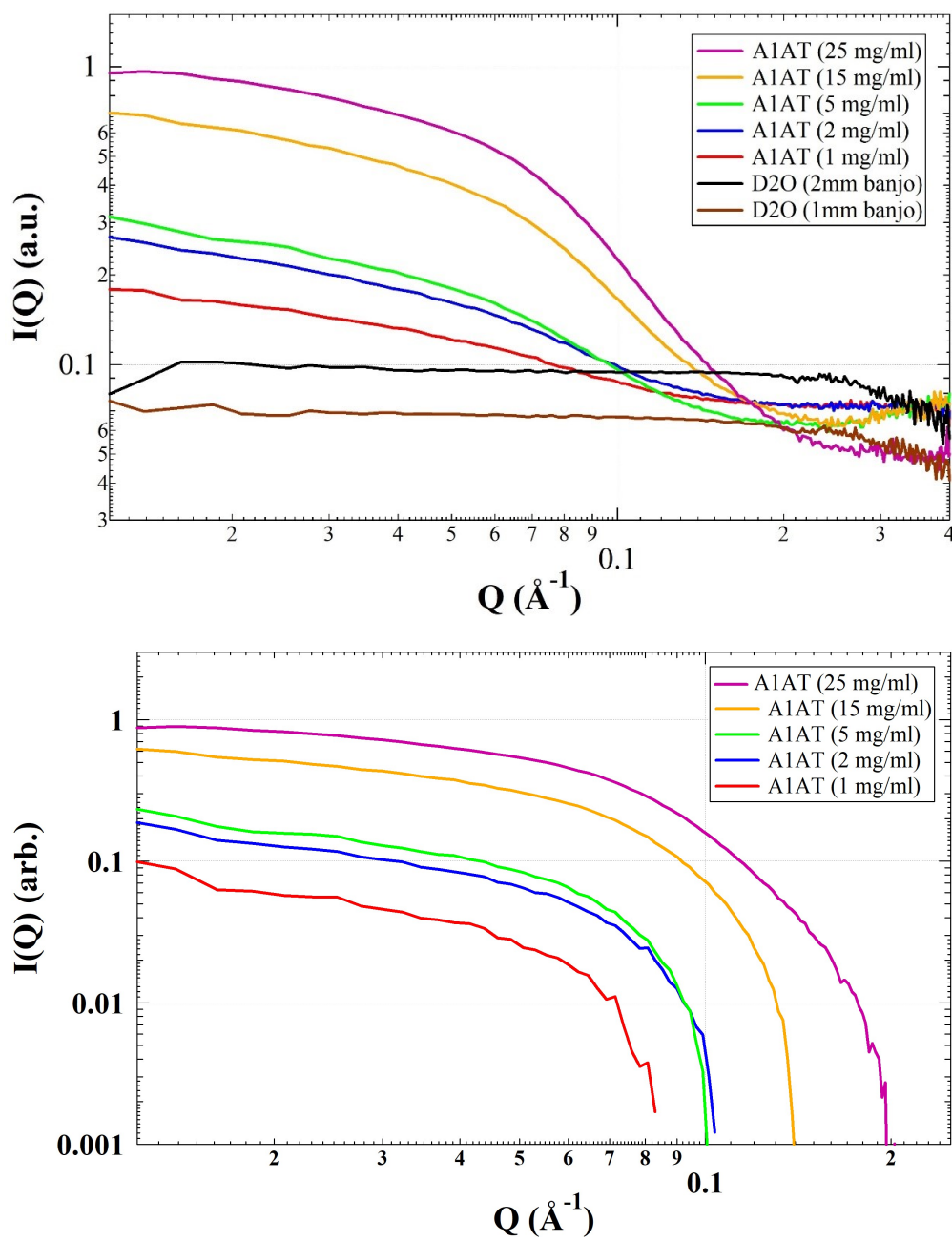


Fig. 4.3. SANS of A1AT in D₂O 1xPBS. Experiments done at EQ-SANS beamline at ORNL-SNS.

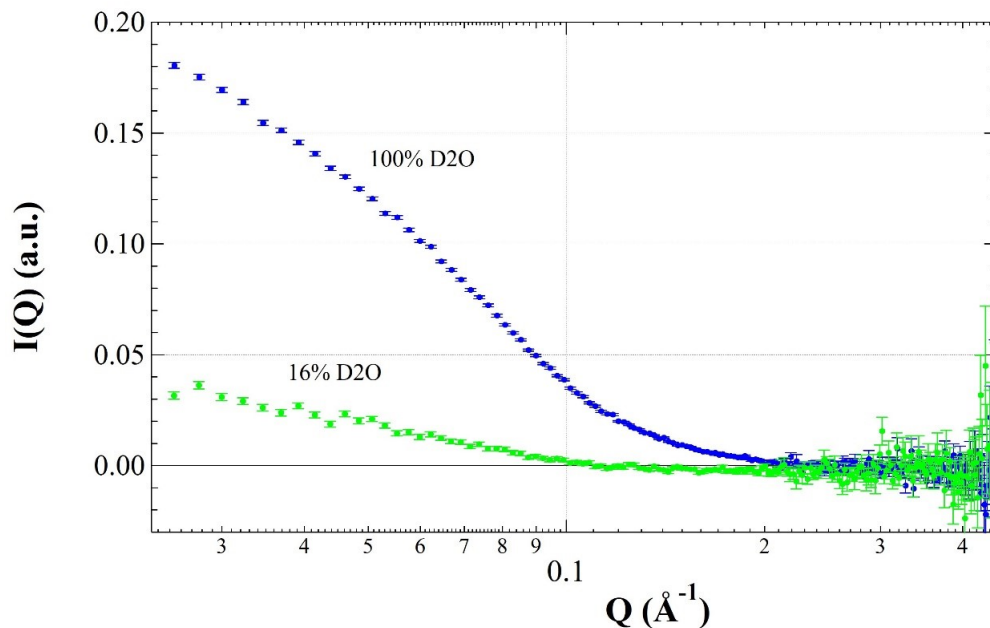


Fig. 4.4. SANS of A1AT in solution at different D₂O/H₂O ratios.

lower concentrations (1 to 15 mg/ml) the $P(r)$ curves show a pronounced lobe centered around 30 \AA as well as local maxima around 90 \AA and at 120 \AA . The secondary maxima could be due to protein aggregation as these distances are multiples of the first peak which shows the population of mostly diluted A1AT units.

Model analysis of scattering data provides values for the radius of gyration of scattering units. These results are shown in Fig. 4.6 for 3 different models considered: calculation from $P(r)$, a Guinier model, and a Guinier-Porod model. Models converge at higher concentrations and diverge at lower concentrations most likely due to low scattering at low protein concentration.

Additional analysis can be performed using various shape models. Results are shown in Fig. 4.7 for spherical, elliptical cylinder, and ellipsoidal shapes. This type of analysis provides geometrical parameters of the shapes used as opposed the R_g values. Fig. 4.7 shows the volumes of scattering units that allows a comparison of

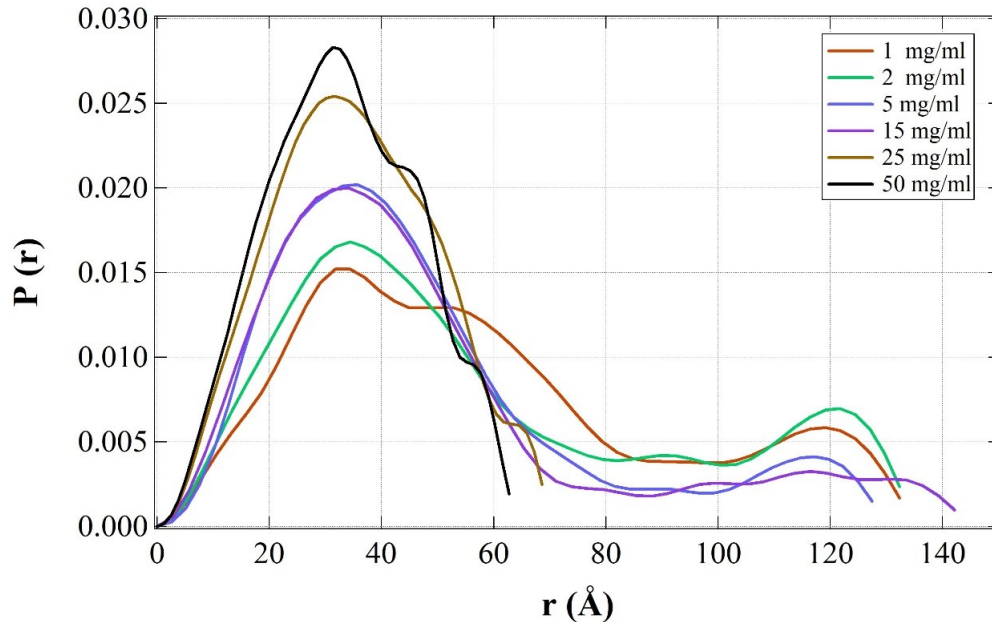


Fig. 4.5. Patterson functions (pair distance distributions) for the A1AT concentration series obtained from SAXS.

different shapes. In order to compare with R_g values obtained before, the volume of a uniform solid sphere as a function of R_g is

$$V = \frac{4\pi}{3} \left(\sqrt{\frac{5}{3}} R_g \right)^3. \quad (4.1)$$

A spherical volume $V \approx 150,000 \text{ \AA}^3$ corresponds to $R_g \approx 26 \text{ \AA}$ indicating consistency between the different models except for the ellipsoidal shapes.

Results can be compared with calculated SANS curves using the crystal structure. This is shown in Fig. 4.8 and which yields an anticipated $R_g = 21.2 \text{ \AA}$. Guinier fits to the scattering data shown in Fig. 4.4 yield $27.1 \text{ \AA} \pm 0.35 \text{ \AA}$ for the 16% D_2O sample, and $22.8 \text{ \AA} \pm 0.035 \text{ \AA}$ for the 100% D_2O sample. The 4.3 \AA difference between the two results is not clear, however, the lower R_g value is more consistent with the theoretical expectation.

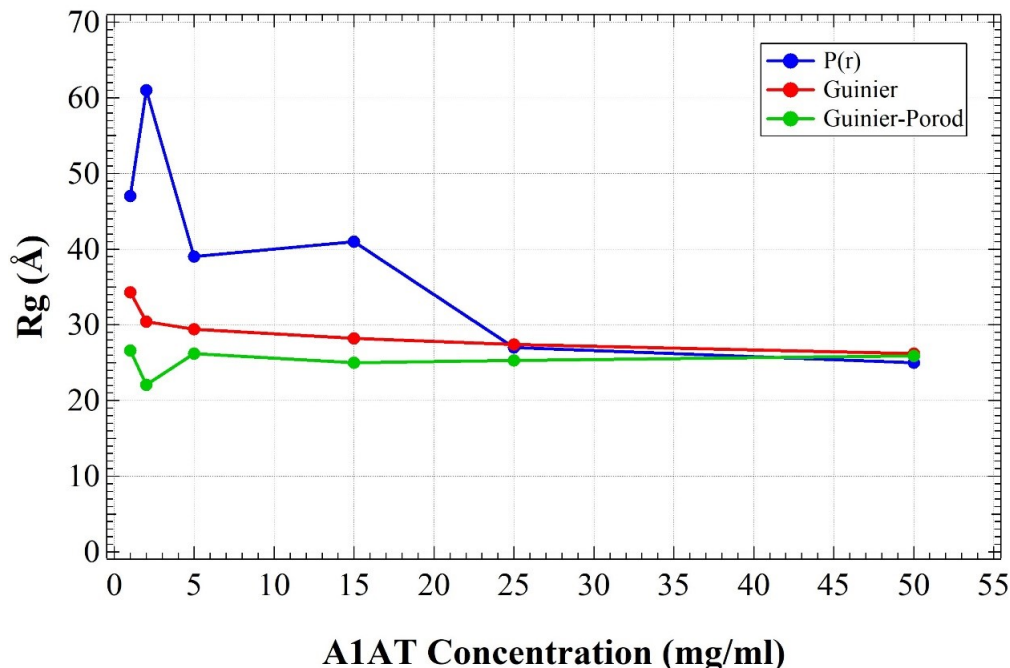


Fig. 4.6. SAXS Analysis of R_g using different models for the concentration series of A1AT samples.

4.2 A1AT under osmotic pressure

Measurements under osmotic stress can provide additional structural information [67, 78, 79]. The best experimental method to apply a well-controlled osmotic stress is by using polymers such as PEG at known concentration. The higher the polymer concentration, the higher the osmotic pressure applied on the protein. For each type of polymer one usually has a choice for the range of molecular weights (MW) to be used. Lower MW polymer, such as PEG 400 has the advantage that high osmotic pressures can be achieved at relatively lower polymer concentration. The disadvantage is that smaller polymer units might intercalate with the protein. Larger MW polymer, such as PEG 20000 is usually used with membranes due to exclusions effects (lack in intercalation) between scattering units. However, solutions of large MW polymers are very viscous and gel-like making sample preparation and homogenization very

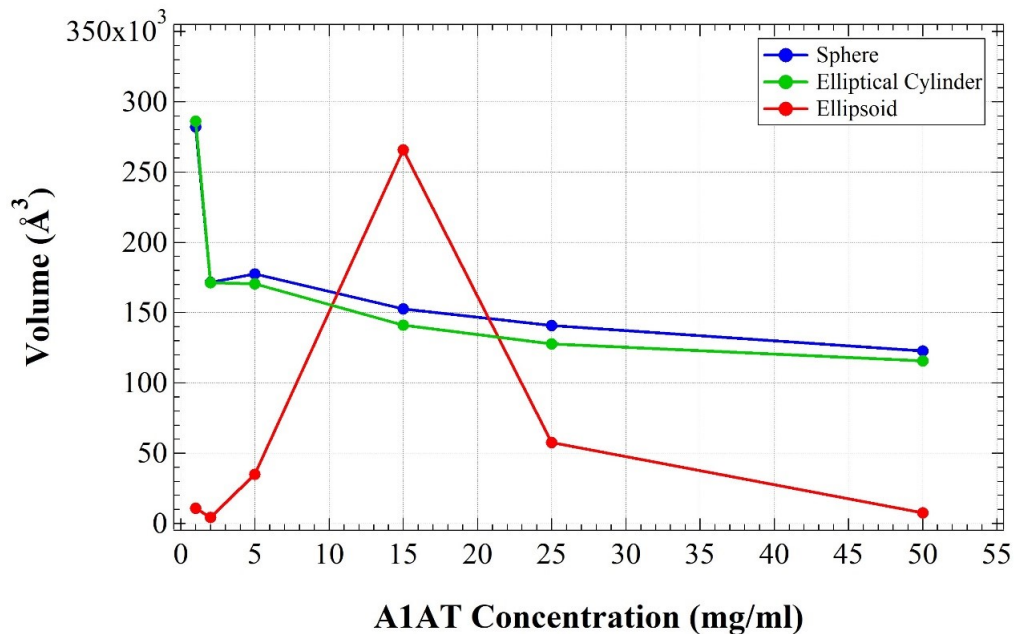


Fig. 4.7. Volume analysis of A1AT for three different shape models.

difficult. For this work, we have use PEG 1500 as a compromise. However, even for this intermediate MW, we found that A1AT samples had to be pre-diluted before adding them to PEG solutions. Sample preparation was done by first diluting the A1AT in water and then mixing the A1AT in solution with PEG in solution at 30°C. Fig. 4.9 gives an example of a comparison between sample preparations that used pre-diluted A1AT in water and preparations without pre-dilution (A1AT powder added directly to PEG solutions).

SANS scans of samples made without pre-dilution were lacking the expected protein scattering at low Q . For this reason, all samples used for data analysis were prepared with pre-dilution. Fig. 4.10 shows SANS data of pre-diluted A1AT under osmotic stress.

The corresponding R_g values using Igor Pro Guinier fits are shown in Fig. 4.11. R_g values decrease as the PEG concentration increases to about 35% after which it increases abruptly at 40% and 50% PEG. This result shows that the effect of osmotic

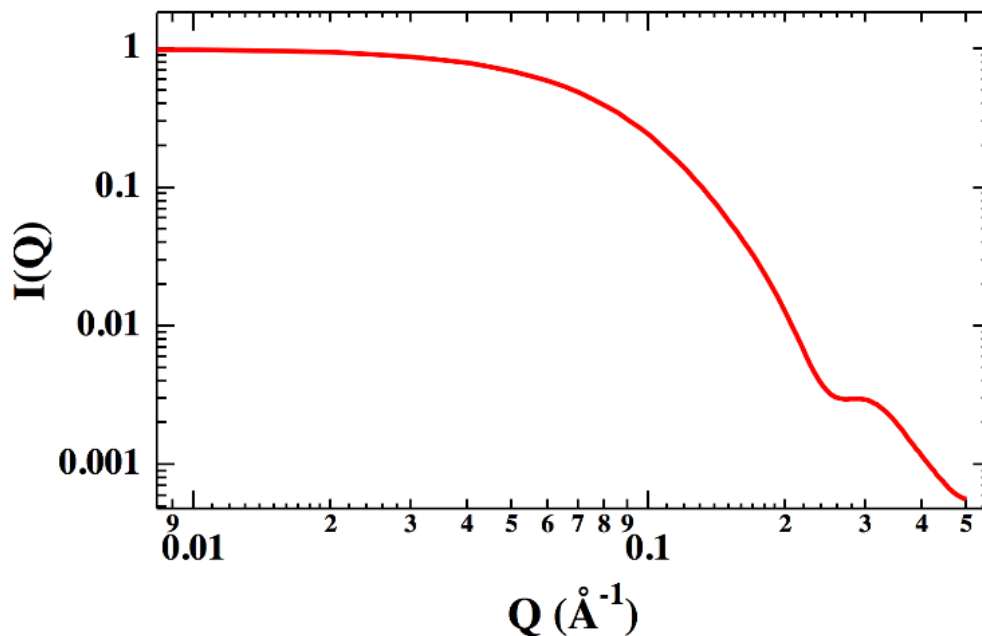


Fig. 4.8. Calculated SANS curve for A1AT using the x-ray crystal structure (2QUG) and the program CRYSON.

pressure is to initially compress the A1AT structure without inducing aggregation followed by aggregation at high osmotic pressure. The measured aggregation threshold at 30% PEG corresponds to the osmotic pressure value where the effect of protein-protein attraction overcomes entropic effects.

SAXS also detects the effect of osmotic pressure on A1AT structures. These are shown in in Fig. 4.12. Although the general trend is similar to SANS data, the analysis of SAXS data for these samples did not give consistent results. This can be due primarily to the fact that SAXS samples are much smaller than SANS samples and therefore SAXS is more prone to sample inhomogeneity than SANS. Complications also arise due to the viscosity of PEG solutions which can create more serious artifacts for smaller samples.

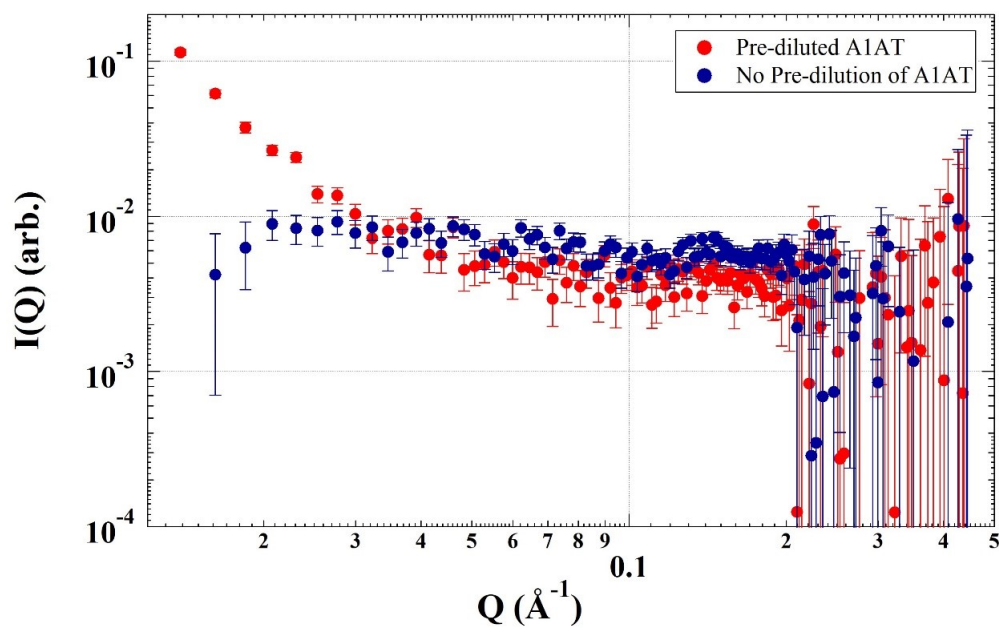


Fig. 4.9. SANS of A1AT in 50 wt% of PEG 1500.

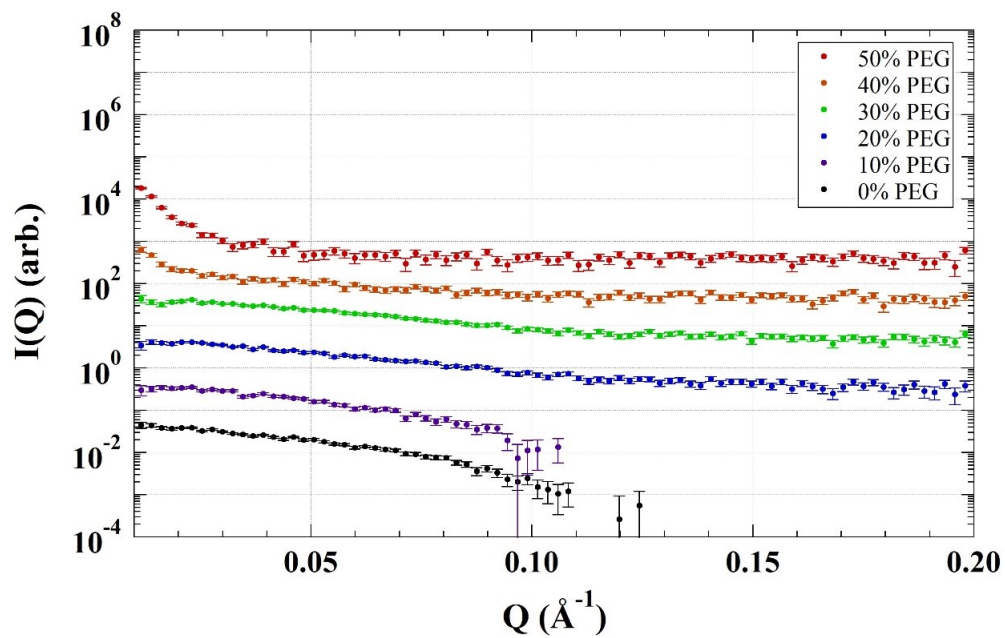


Fig. 4.10. SANS of pre-diluted A1AT under osmotic stress at 30°C .

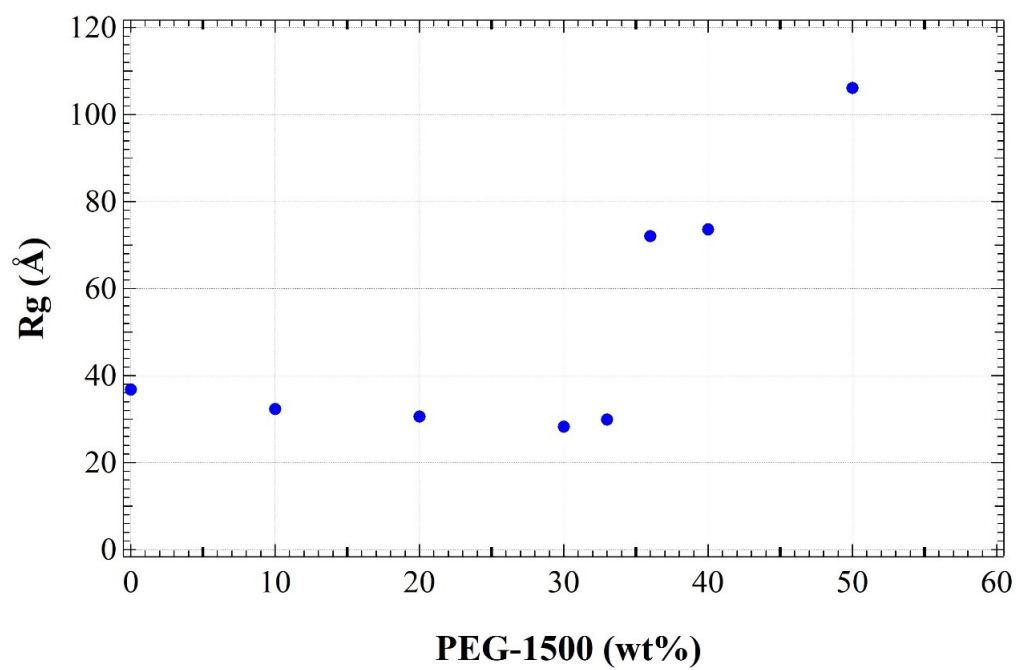


Fig. 4.11. Radius of gyration of A1AT as a function of PEG concentration as determined from SANS data using Igor Pro Guinier fit.

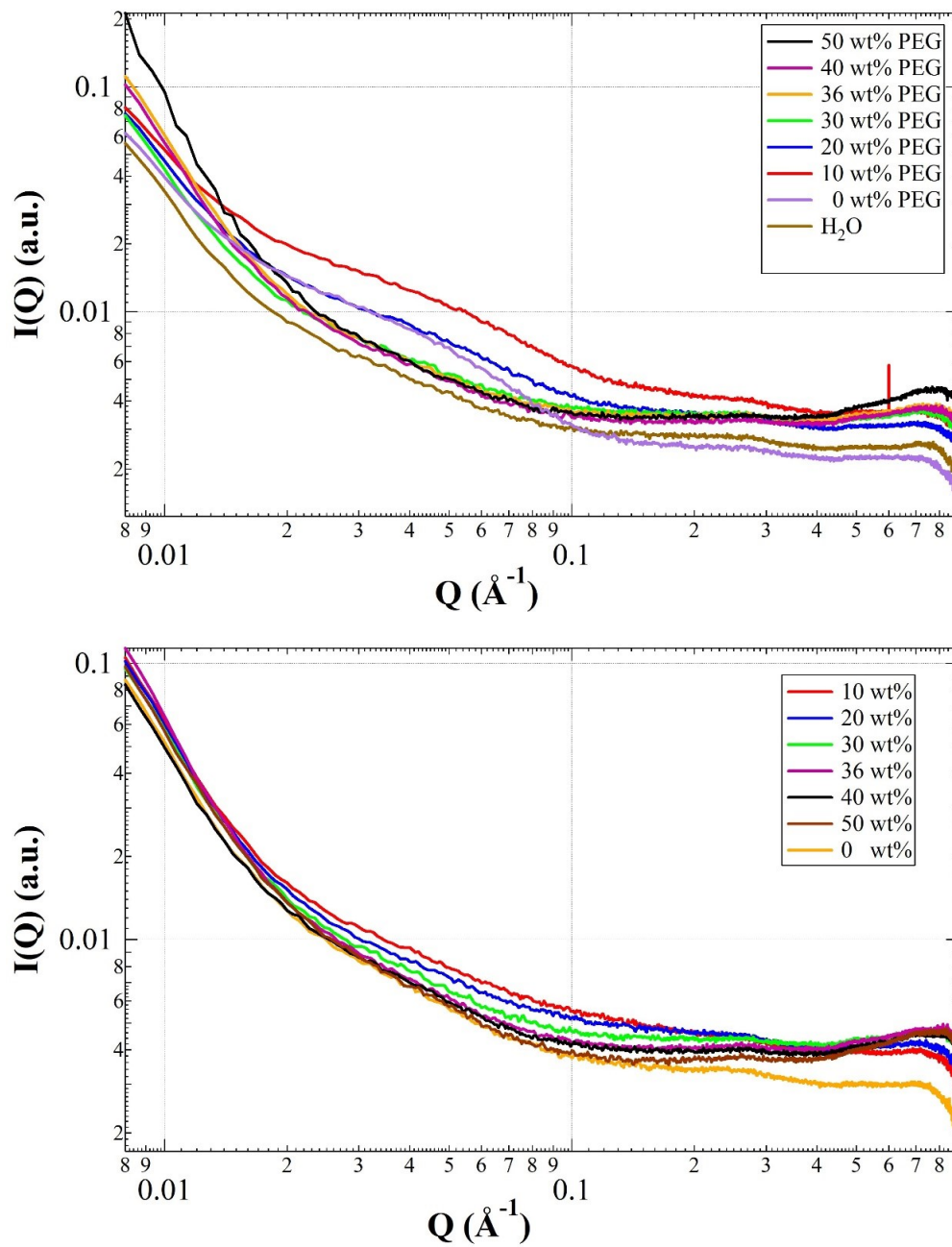


Fig. 4.12. SAXS measurements of A1AT in PEG 1500 solutions (upper panel) and background scans (lower panel).

4.3 A1AT and lipid

Scattering measurements of A1AT were also performed in the presence of lipid vesicles to see if we can obtain aggregate materials in which the protein is incorporated into lipid structures. Ion channel measurements in the lab that were not part of this thesis project have showed that A1AT proteins affect the activity of gramicidin A ion channels with a stronger affect for the negatively charged PS lipids compared to neutral PC.

The approach for this study was the following. Because PC lipids in water form multilamellar vesicles scattering measurements show characteristic Bragg peaks corresponding to the lamellar repeat (D -spacing). For POPC in water at 30°C, there are two Bragg peaks, one around $Q = 0.1 \text{ \AA}^{-1}$ and the other at $Q = 0.2 \text{ \AA}^{-1}$. Because there is no significant lipid scattering below $Q = 0.1 \text{ \AA}^{-1}$ the protein scattering at low Q can be distinguished from the lipid signal. By changing the amount of lipid and protein, we can therefore investigate two main features of the scattering curves: 1) the relative scattering intensity of protein and lipid, and 2) possible shifts in the location of lipid peaks. By observing these aspects we can determine if the A1AT protein and the POPC lipid form mixed compounds.

The SAXS profiles in Fig. 4.13 show distinct scattering from the protein at lower Q values (less than 0.1 \AA^{-1}) and from lipid vesicles at larger Q values, as expected. POPC lipids in water form multilamellar structures that typically exhibit two relatively sharp scattering peaks as seen in Fig. 4.13. For pure POPC in water, these peaks are narrow and sharp and the top of the peak is essentially Gaussian. However, when pH buffers are present as in these sample, peak line-shapes became more complicated due to a coexistence of lamellar phases as described in [80].

The data in Fig. 4.13 show that scattering at low Q increases in proportion to the amount of A1AT protein in the sample and at the same time leaving lipid peaks unaffected. The most likely situation consistent with such a behavior is a complete separation of lipid and protein phases.

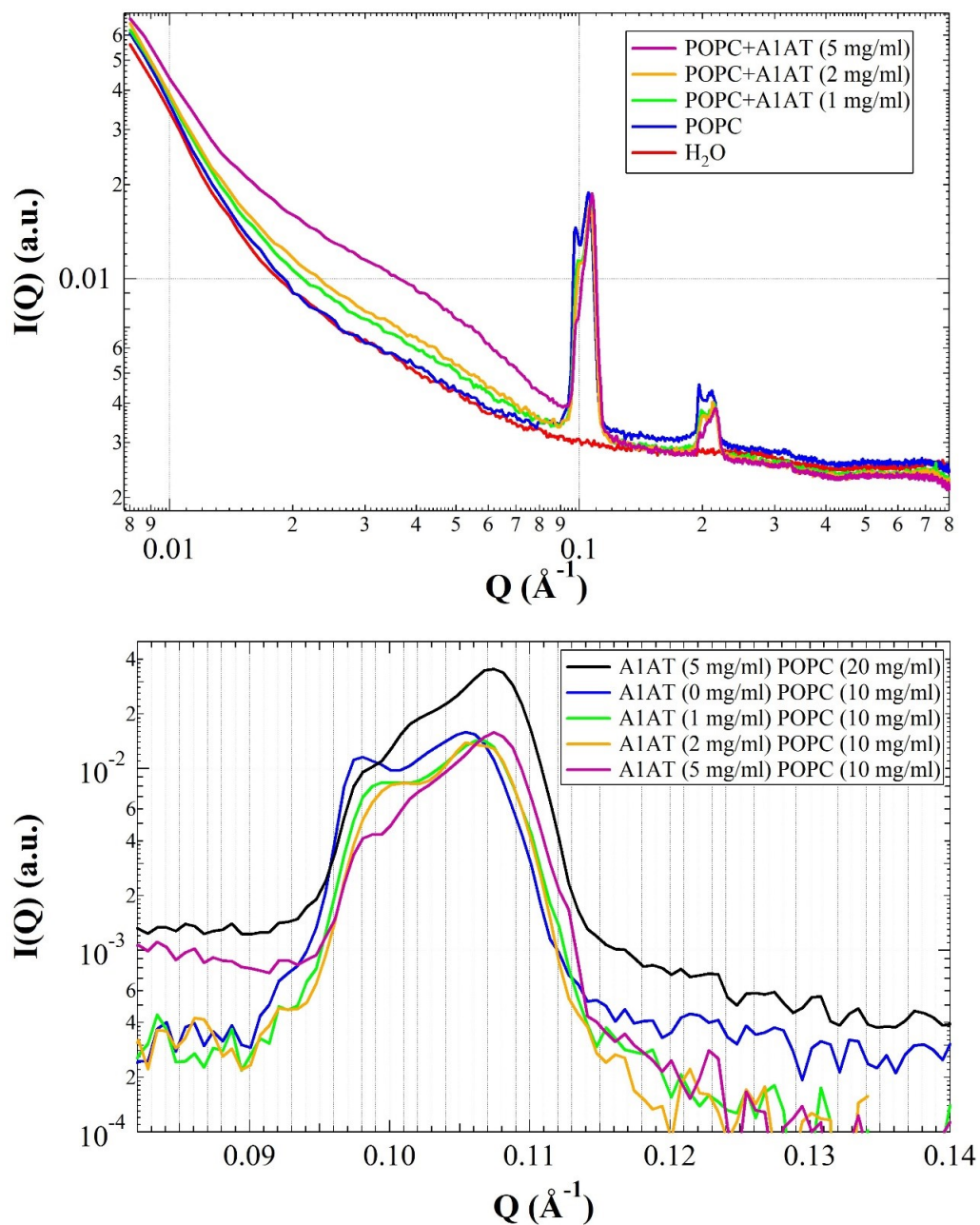


Fig. 4.13. SAXS measurements of samples containing A1AT protein and POPC lipid vesicles in H_2O 1XPBS solution at 30°C . The upper panel shows the full measured range while the lower panel zooms on the 1st lipid peak.

A similar conclusion is reached based on SANS measurements as shown in Fig. 4.14. No significant difference is observed in the lipid peak when comparing the scattering with and without A1AT in D₂O/H₂O solutions chosen to match the scattering length of the protein.

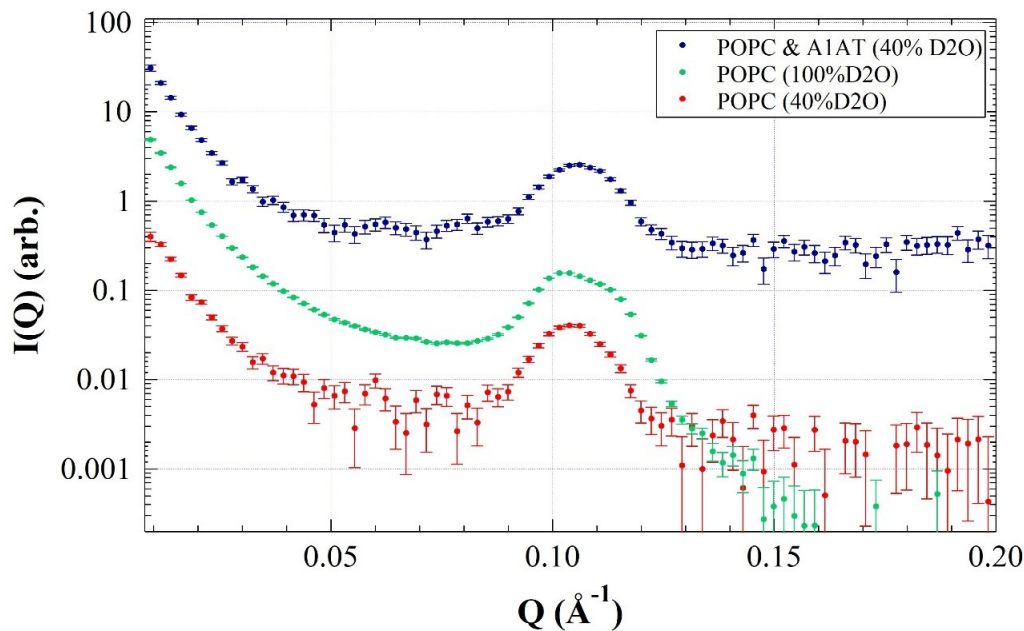


Fig. 4.14. SANS measurements of A1AT+POPC samples in 40% D₂O/H₂O mixture and of POPC alone in 40% D₂O/H₂O and in 100% D₂O .

Measurements of A1AT in the presence of the negatively charge POPS lipid are shown in Fig. 4.15 and Fig. 4.16 for SAXS and SANS, respectively.

Both sets of data indicate that A1AT affects the scattering profile of POPS. As opposed to POPC which forms multilamellar structures, the electrically charged POPS tends to form unilamellar lipid vesicles. For this reason, POPS scattering shows a broad scattering feature in the range $.1 \text{\AA}^{-1} - .2 \text{\AA}^{-1}$ as seen in the figures. Depending on the buffer solution and sample geometry, single vesicles can be found in coexistence with a small fraction of multilamellar vesicles that produces Bragg peaks. Addition

of A1AT reduces the amplitude of the broad lipid feature indicating mixing of POPS single vesicles with A1AT.

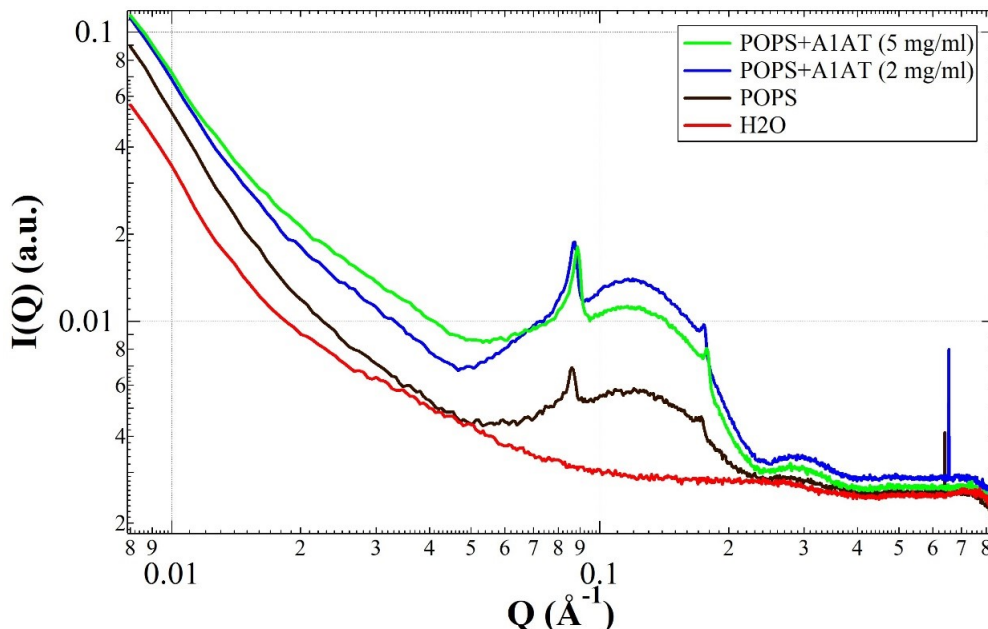


Fig. 4.15. SAXS of POPS lipid and of POPS with A1AT.

Fig. 4.16 shows SANS of POPS in solution, and of POPS with A1AT while matching protein to the background to observe POPS.

Measurements were also performed in the presence of DLPC lipid. DLPC is not as biologically relevant as POPC but it is often used in measurements of membrane interactions because it tends to give sharper scattering peaks than POPC under a wide variety of conditions. Fig. 4.17 shows SAXS measurements of A1AT in the presence of DLPC multilayers at $T = 30^\circ \text{C}$.

Although the amplitude of the lipid peak changes, this change is not systematic with the amount of A1AT, rather, we attribute this variation to variations in the amount of lipid material localized in the x-ray beam.

We conclude that A1AT has a measurable effect in the scattering of PS and either no effect (or under experimental detection limit) for the case of PC lipids.

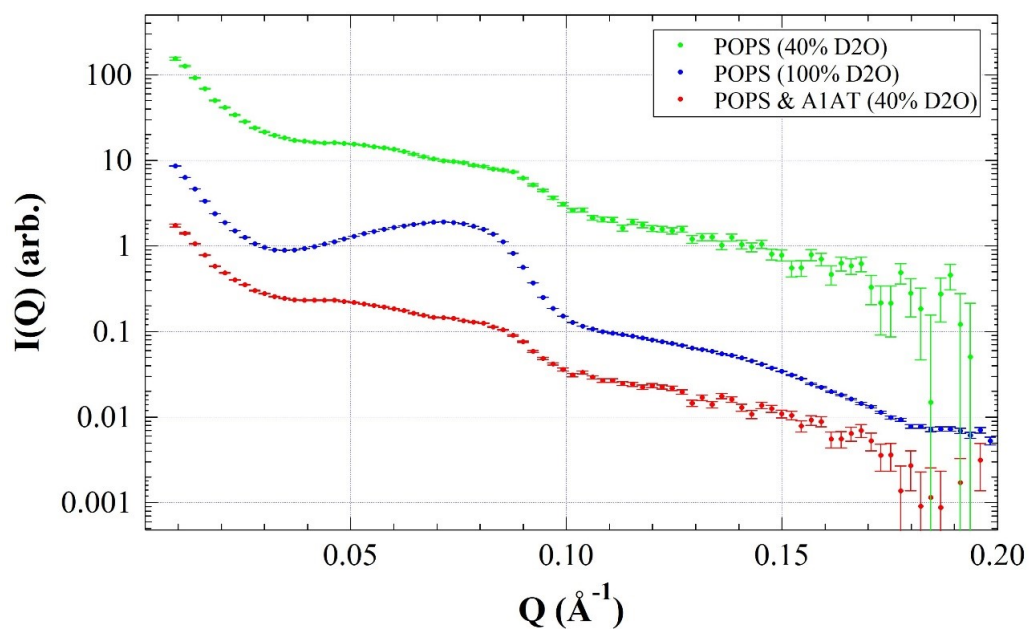


Fig. 4.16. SANS of POPS in solution, and POPS with A1AT while matching protein to the background to observe POPS.

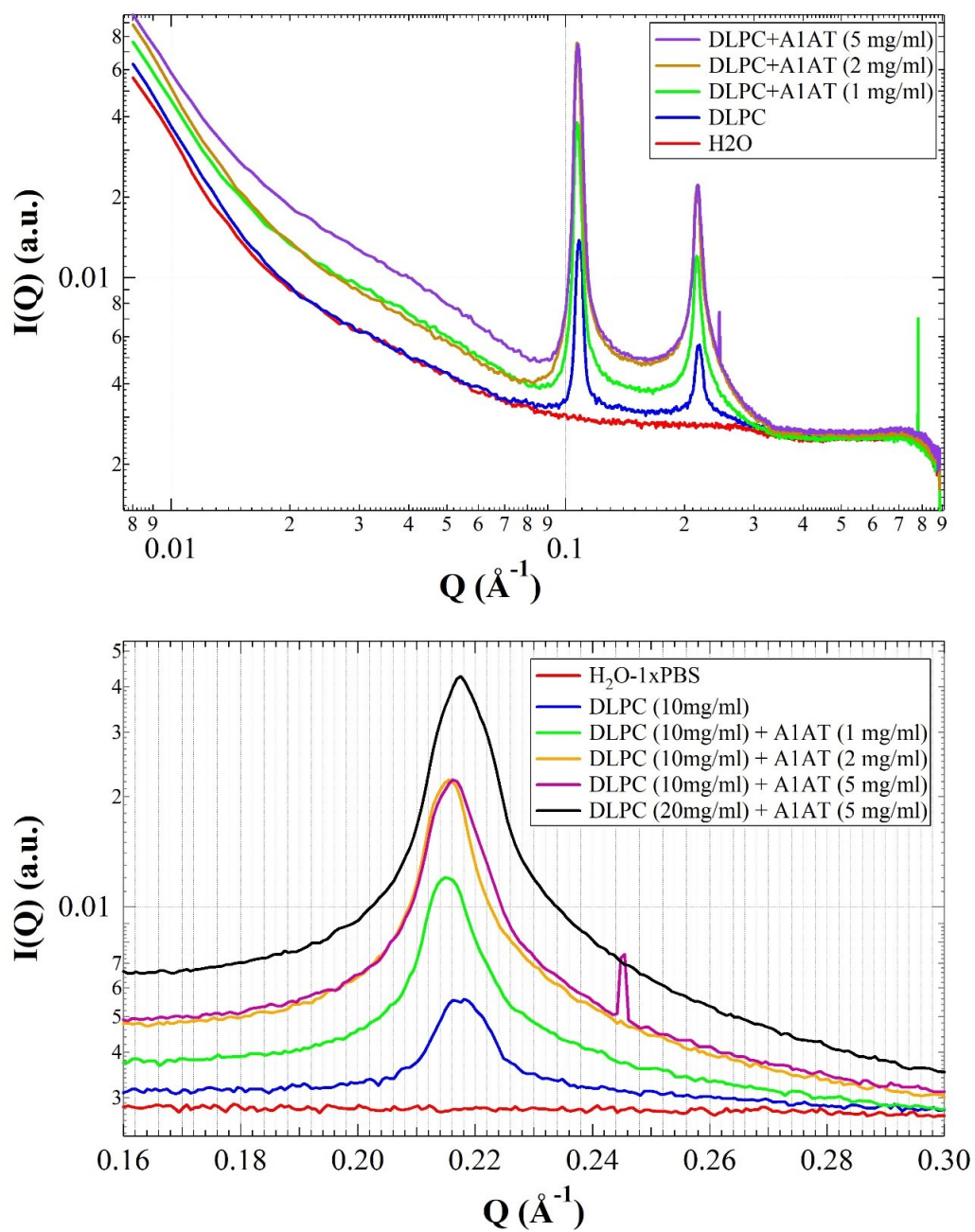


Fig. 4.17. SAXS measurements of samples containing A1AT protein and DLPC lipid vesicles in H₂O 1XPBS solution at 30°C. The upper panel shows the full measured range while the lower panel zooms on the 2nd lipid peak.

4.4 Fibrin polymerization

Fibrin measurements in this thesis were performed by SANS and by Dynamic Light Scattering (DLS) as a function of time. Experiments were done using near physiological concentrations of fibrinogen and thrombin (4 mg/ml to 5 mg/ml of fibrinogen and 1 unit/ μ l of thrombin) and the goal was to follow the polymerization reaction in real time. The detector used at the BL6 (EQ-SANS) allows the user to accumulate scattering data over a long period of time and then go back and extract specific time windows for analysis. EQ-SANS was set to use two wavelengths: 2.5 Å and 10 Å, in order to capture a wider Q range. This arrangement allows the user to better monitor the dynamic of protein polymerization growth. Two methods were employed: the two wavelengths were used simultaneously (using frame skipping) when capturing the dynamic evolution of the polymerization; and the two wavelengths use one after the other (2.5 Å, then 10 Å) to capture a higher resolution picture of the initial portion of the polymerization, while using the longer wavelength to capture the end state of the polymerization. The scattering profiles shown in Fig.4.18 correspond to 5 minute windows starting at the timepoints indicated by the labels, that is 5 to 10, 10 to 15, 15 to 20, and the 68-73 min, where 73 minutes was the total duration of the scan. In the experiment, each measurement was set to a target number of counts and therefore the exposure time was dependent on the state of the incident neutron beam. The scattering profiles in Fig.4.18 are almost identical indicating that no detectable structural changes occur after the first 5 minute interval. The only possible explanation is that the polymerization reaction happened at a shorter time scale.

In order to investigate reaction times in various conditions, we have performed Dynamic Light Scattering (DLS) experiments. These are less powerful and less accurate for measurements of polydispersed samples but more affordable than SANS. These DLS measurements were performed to find the time scale of the polymerization reaction in at various fibrinogen and thrombin concentrations in solution in order to

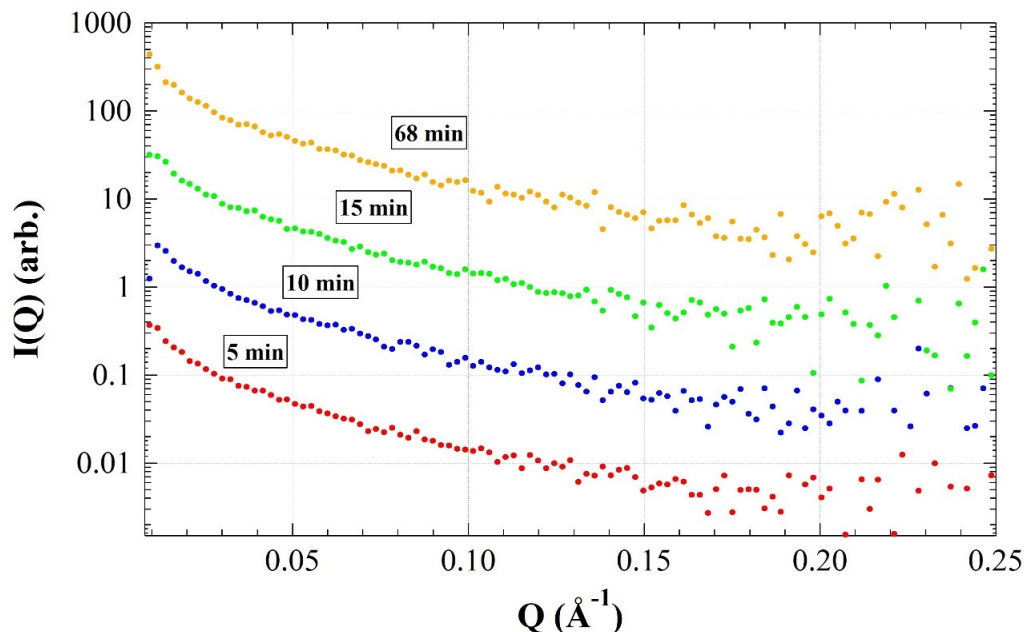


Fig. 4.18. SANS of fibrin polymerization using 5 mg/ml fibrinogen and $1\mu\text{l}$ of Thrombin (1 unit/ μl), in 80% D_2O solvent). Each profile is accumulated over 5 minute time windows starting at the timepoints indicated by the labels.

optimize the analysis of SANS data and to design future experiments. The EQ-SANS (BL6) instrument at ORNL was used to redo the time resolved SANS experiments using the following concentrations: fibrinogen at 0.4 mg/ml and $0.1\mu\text{l}$ of thrombin (1 unit/ μl). DLS was used to determine the range of protein concentration for SANS experiments. Using 4 mg/ml fibrinogen and 0.01 u/ml thrombin yields about 90 minutes of reaction time. Measurements are shown in Fig. 4.19.

The DLS results indicate that fibrin polymerization completes in less than 10 minutes in our samples which unfortunately is too short for SANS. Although apparent changes in size continue to occur even after 30 minutes, we attribute this to sedimentation of large fibrin particles which are no longer in the path of the laser beam.

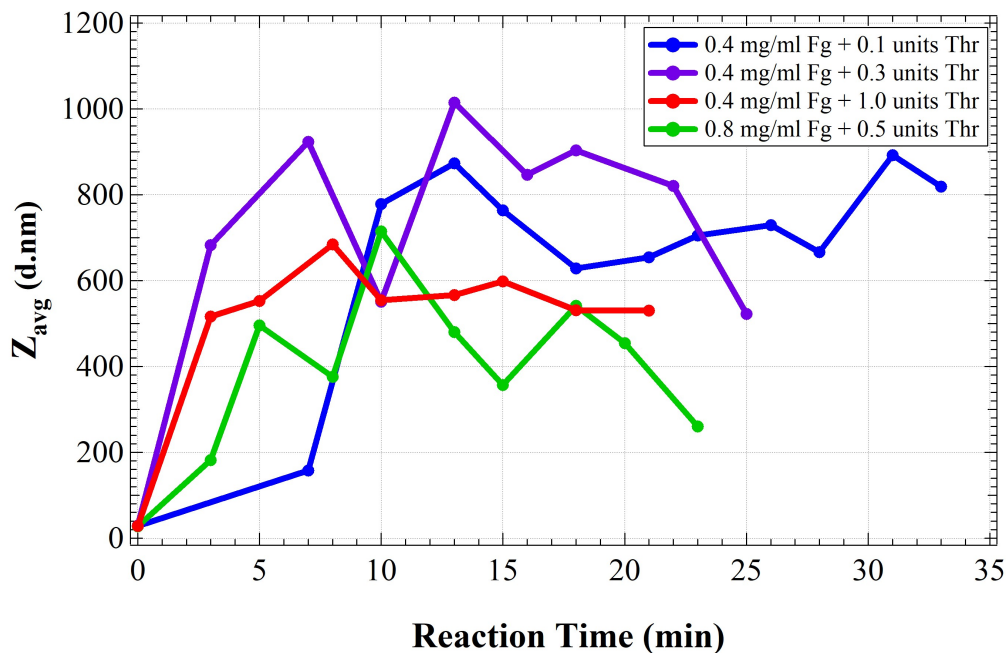


Fig. 4.19. Average size (diameter) of fibrin particles measured by DLS as a function of time. Different curves correspond to different amounts of fibrinogen (Fg) and thrombin (Thr) enzyme in the sample.

Fig. 4.20 shows another set of time resolved SANS measurements of Fibrin polymerization (4.25mg/ml Fg, 0.01 units/ml Th) in 1XPBS, 80% D₂O .

Because of its larger size, the analysis of polymerized fibrin using standard methods is more complicated than for A1AT. Fig. 4.21 shows PDF of time resolved (PDF of Fibrin Formation Kinetics: Monodisperse System of Rod-like Particles) SANS measurements shows how the cross section of Fibrin changes as a function of time. The analysis has been performed using GNOM.

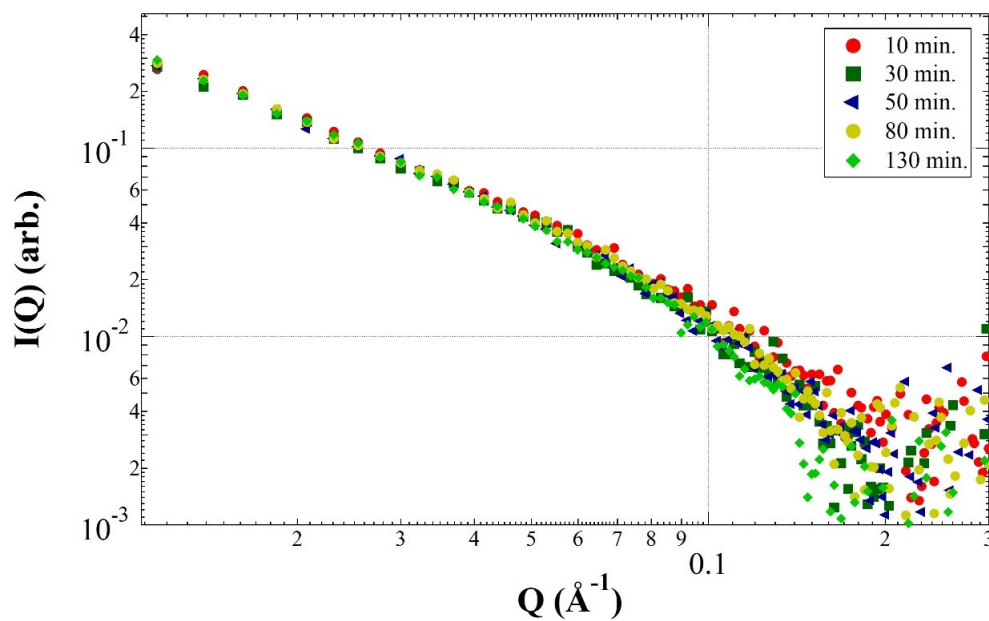


Fig. 4.20. SANS of fibrin polymerization using 4.25 mg/ml fibrinogen and 0.01 μl of Thrombin (1 unit/ μl), in 80% D_2O solvent). Each profile is accumulated over various time intervals as shown on the legend.

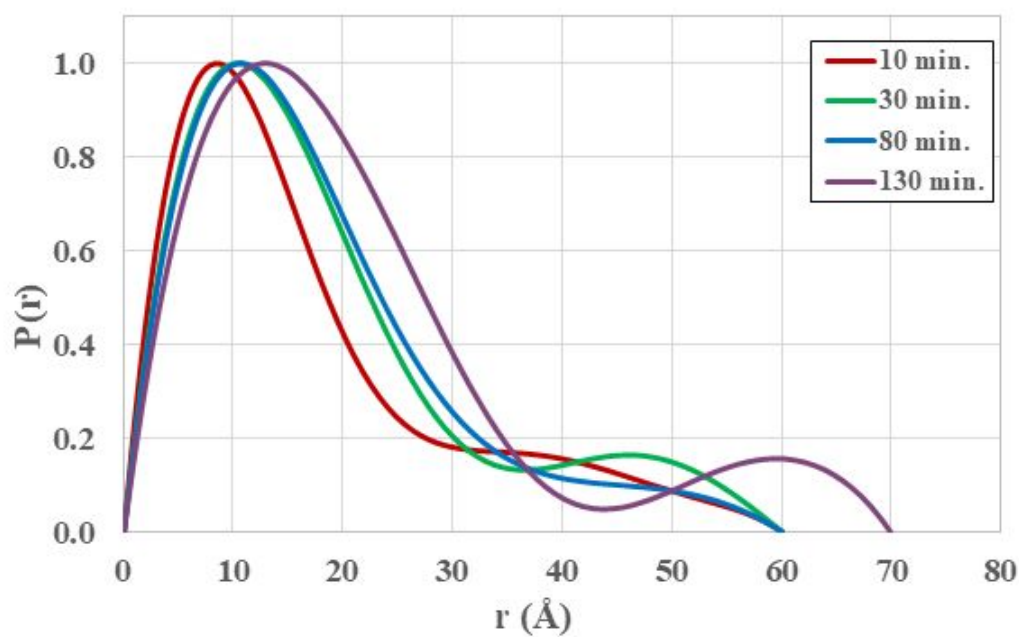


Fig. 4.21. PDF of Fibrin Formation Kinetics obtain from a GNOM analysis.

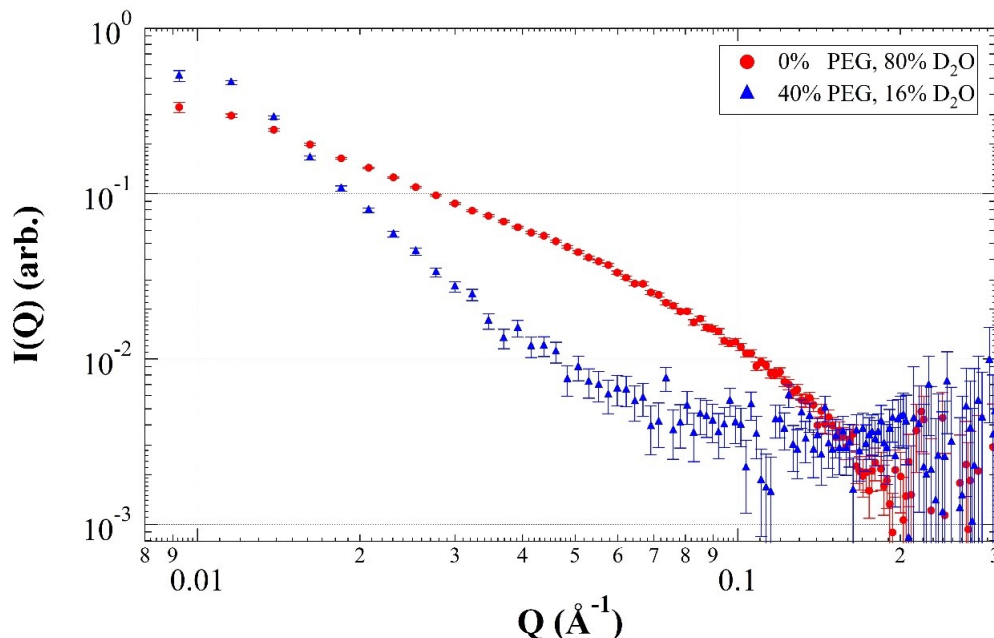


Fig. 4.22. SANS profiles for fibrinogen in water and in 40% PEG 1500.

4.5 Fibrinogen under osmotic pressure

Fig. 4.22 shows that osmotic pressure has an effect on fibrinogen polymerization. The more abrupt decay of the scattering profile with increasing scattering angle indicates larger aggregates in the presence of PEG. Note that the profile in the presence of PEG is similar to those of polymerized fibrinogen in the presence of thrombin enzyme.

PDF analysis of fibrinogen scattering under osmotic stress using GNOM and using either a monodispersed system of rod-like particles or sphere-like particles are shown in Fig.4.23. These PDFs show how osmotic stress affects the size and structure of Fibrinogen's envelope shape, when treated as a particle.

The analysis is done using the Large Scale Structure analysis procedure which gives the distance distribution function of the cross-section assuming monodisperse system of rod-like particles. The function $P(r) = \gamma_c(r) * r$ is evaluated, where $\gamma_c(r)$ is

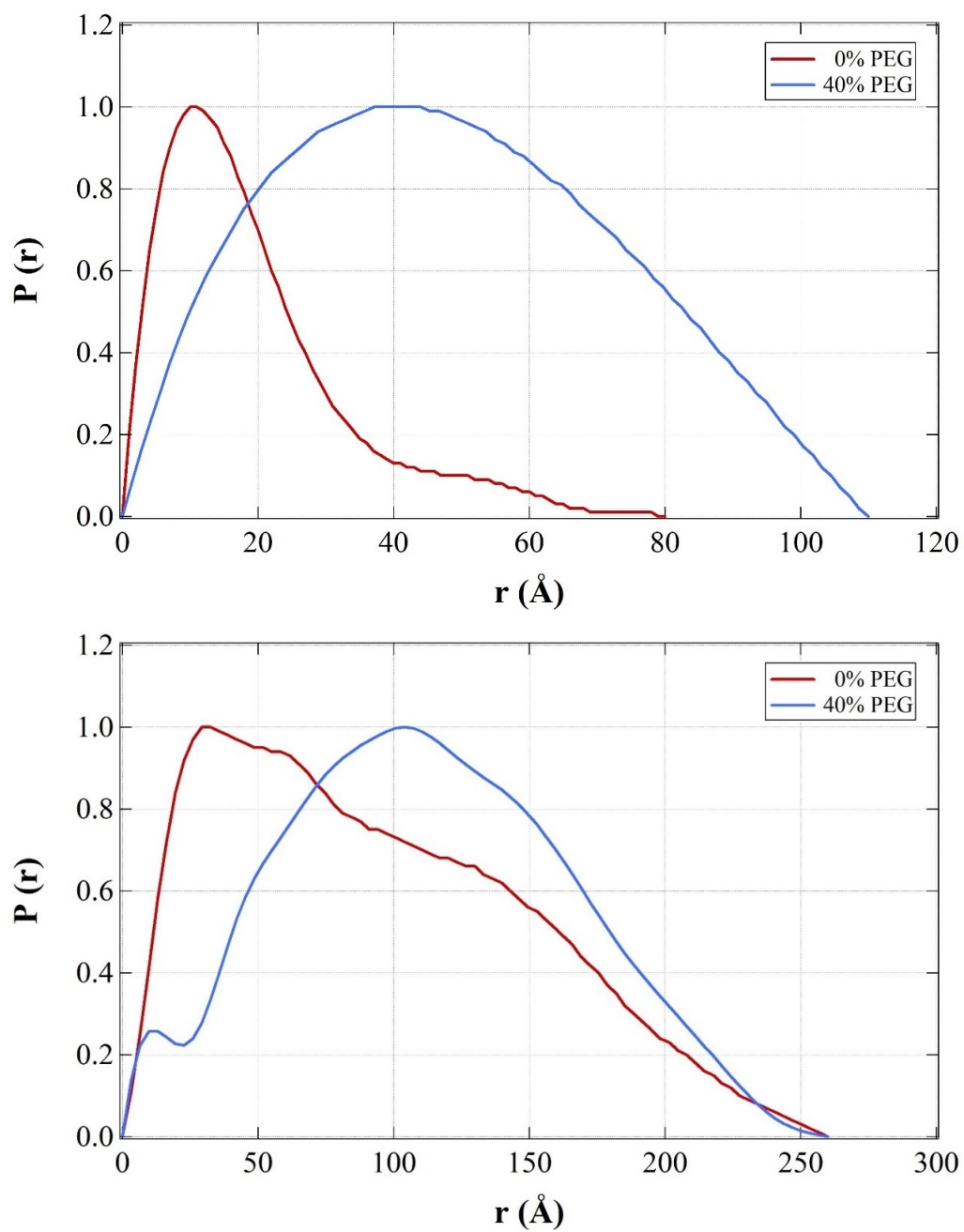


Fig. 4.23. Analysis of fibrinogen under osmotic stress using GNOM for a rod-like model (upper panel) and a sphere-like model (lower panel).

the characteristic function of thickness. In this case the experimental intensity as well as the errors are multiplied by s , which corresponds to the cross-section scattering factor.

5. DISCUSSION

For proteins in solution, scattering methods do not provide a 3D atomic structure as one might obtain from computer simulations either alone or in combination with solution NMR measurements. Instead, scattering methods as presented in this work can give information on structural variations due to changes in external conditions. Scattering methods can also be an indirect but efficient way of identifying molecular affinities, miscibility, and possible coexistence of phases as in the study of A1AT interacting with lipid vesicles.

Fibrinogen and Alpha 1-Antitrypsin (A1AT) are plasma glycoproteins with different, but specific biological functions. A1AT has been shown to have protective roles of lung cells against emphysema, while fibrinogen is a major factor in the blood clotting process. Most known glycoproteins have been shown to play a role in cellular interactions but the exact role of the glycan chains which are not visible to small-angle scattering is still under investigation.

The main questions addressed through the measurements presented in this thesis are the following: 1) What structural changes of large protein aggregates take place either as a function of time or under osmotic pressure? 2) How do large protein structures interact with lipid vesicles? and 3) Can we monitor and optimize polymerization conditions for proteins such as fibrinogen?

The motivation for 1) and 3) was due to questions regarding the ability to observe structural changes in large molecular aggregates by standard scattering methods. The motivation for the 2nd aspect is due to observations of A1AT interaction with lipid membranes used in ion channel measurements in our laboratory (data not shown). It was observed that A1AT affects gramicidin ion channels more when embedded in phosphatidylserine (PS) lipid bilayers than in phosphatidylcholine (PC).

A major aspect of this work is finding optimum sample preparation protocols. As shown above, due to sample inhomogeneity, there is a non-trivial effect of sample history which is more pronounced for fibrinogen than for A1AT due to its larger size. There are also noticeable differences between SAXS and SANS results which arise primarily for two reasons. One is that the time scale of the measurement with scan times on the order of a second or less in the case of SAXS compared to half an hour for SANS. The second reason for the observed differences is the relationship between the cross-section of the beam and the sample physical size. Synchrotron x-ray beams are on the order of a millimeter or less in diameter compared to centimeter for neutrons. This means that SANS sees a much larger fraction of the sample compared to SAXS. In combination with longer exposure times, SANS data then correspond to averaging over inhomogeneities to a much larger degree than in SAXS. For this reason, it was found that in the case of fibrinogen, SANS measurements needed to be supplemented with DLS measurements which are both faster and operating at larger length scales.

For A1AT, we find that a structural transition occurs under osmotic stress applied using PEG. This transition is between 33 wt% PEG and 36 wt% PEG in solution, when fitting for the radius of gyration using Guinier fit (Igor Pro; ORNL package). There are two regions of linear relationship between R_g and PEG concentration. It is also worth noticing that the jump in R_g after 33% is about double, and then triple for 50% wt% PEG. This can possibly be forced aggregation. This could then be compared to the concentration series to find out if crowding has the same effect, or if the effect of compression and aggregation is not seen even at 50 mg/ml A1AT concentration.

We also found that there was no change in protein structure or aggregation due to changes in protein concentration, within the range explored: 1 mg/ml to 50 mg/ml (Fig. 4.1). Technically however, there was a disagreement between the three different methods used to determine the R_g at lower concentrations (Fig. 4.6) most likely due to a small signal-to-noise ratio at low protein concentration.

A linear fit through the first five data points in Fig. 5.1 that correspond to the protein compression under osmotic stress gives $R_g = -0.2189x + 35.652$, where x

stands for PEG wt%. We can use this linear form to find a theoretical value for PEG concentration that would correspond to the calculated $R_g = 21.2 \text{ \AA}$ for the x-ray crystal structure (2QUG) (Fig. 1.1). The linear extrapolation gives a concentration of PEG of about 66 wt%. Obviously, as shown in Fig. 4.10, the protein does not shrink to this small size under physiological conditions; rather as PEG concentration increases above 35 %, we see a major structural change indicating protein aggregation in larger units which makes it impossible to determine the R_g values for individual protein units.

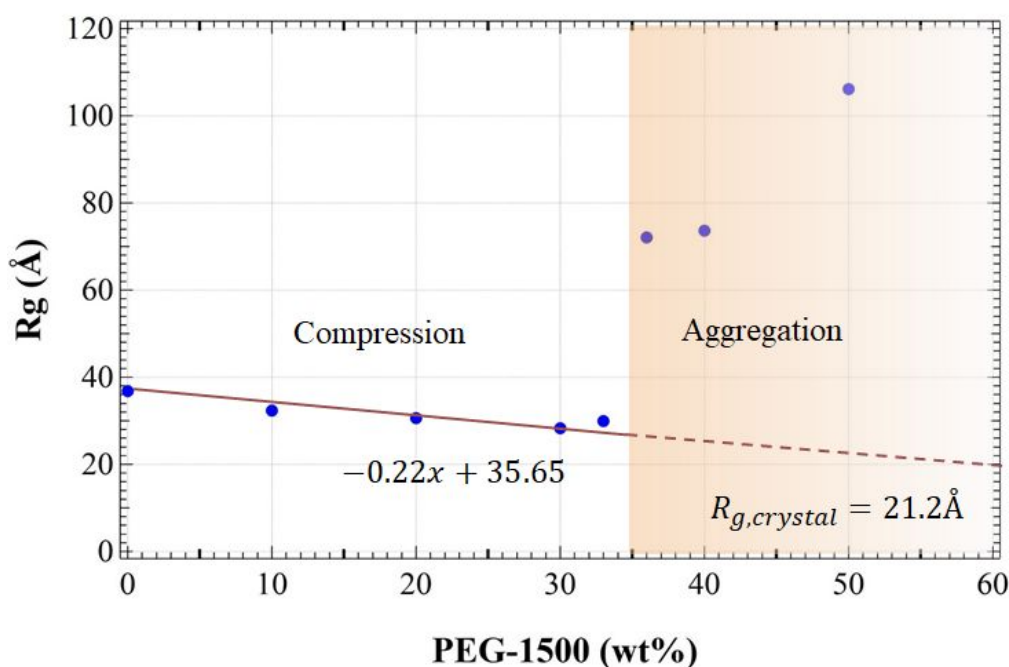


Fig. 5.1. Radius of gyration of A1AT as a function of PEG concentration as determined from SANS data using Igor Pro Guinier fit. The figure shows a linear fit to the compression regime at low osmotic pressure and the shading indicates protein aggregation.

Our analysis also shows that the fitted Q range directly affects the results of the analysis. If the range is not explored to ensure consistency, the results may not be correct or accurate. In this case the range needed a Q_{max} higher than 0.30 \AA^{-1} .

An additional complication for SAXS samples containing PEG and A1AT was due to background subtraction needed to eliminate the contribution from PEG. This was due to the non-linear scattering profile from the gel material formed by PEG when hydrated. In this respect, SANS can be a better method since scattering from PEG can be eliminated (or at least minimized) using contrast matching. The best method for analysis was to match the solvent curve to the full sample curve at a Q range between 0.3 \AA^{-1} and 0.5 \AA^{-1} then subtract the background. A constant background subtraction was needed when doing the analysis in programs other than SasView (as SasView would identify the constant background and account for it), like Igor Pro and GNOM. An accurate background subtraction was not possible when using SAXS for samples containing A1AT and PEG.

Turning to SANS, the measured radius of gyration for A1AT differs between the protein sample in 100% D₂O ($22.8 \text{ \AA} \pm 0.035 \text{ \AA}$) and the sample in 16% D₂O ($27.1 \text{ \AA} \pm 0.35 \text{ \AA}$) and the origin of this 4.3 \AA difference is not exactly clear. It could be due to sensitivity to contrast and therefore an experimental artifact, or it could be due to a change in dynamics (and therefore sample history) as a function of D₂O content.

For both SAXS and SANS, when preparing the samples of A1AT and PEG, it was found that the best method was to pre-dilute each solute individually, then mix the two solutions rather than adding the solutes to the same solvent in one vial. Supernatant was an issue when A1AT was added to PEG in solution which meant that the resulting mixture was not homogeneous.

Sample history turned out to be even more complicated in the case of fibrinogen. [81–84] Under physiological concentrations of fibrinogen and thrombin, it takes between 3 and 5 minutes to form the fibrin network. The challenge to study the formation of a fibrin clot is that SAXS (at Argonne) will produce radiation damage if there is prolonged exposure (more than 100 ms), while SANS (at EQ-SANS) will not capture the kinetic evolution of the formation because it needs at least 15 to 20 minutes of beam time in order to create a sufficient signal to noise ratio. Dynamic

Light Scattering was a necessary method in finding a lower concentration that would yield a 90 minute kinetic evolution of the fibrin clot in order to be captured by SANS.

An interesting finding is the fact that SANS measurements of fibrinogen under osmotic pressure show that the scattering of fibrinogen in 40% PEG but without the thrombin enzyme is similar to that of fully formed fibrin in the presence of thrombin and no PEG. This result suggests a possible research avenue for the analysis of blood clot formation in various physiological conditions in which alteration of solute concentrations in blood and in the extracellular matrix can affect the dynamics of clot formation.

Similarly interesting is the finding that although A1AT does not visibly mix with lipids, SAXS measurements do detect the preference of A1AT to PS lipid compared to PC. This preference can be exploited in possible medical applications using liposomes for supplementing A1AT into the blood stream of patients with A1AT deficiency. Currently, one therapy for the treatment of A1AT deficiency uses blood plasma of healthy human donors to increase the alpha-1 levels circulating in the blood and lungs of patients (a therapy called augmentation therapy.) [49–51,85–90] In principle, pharmaceutical methods could be explored using A1AT complexes with PS lipids.

A more general discussion of protein deformation under osmotic stress can be warranted based on the results presented in this thesis. In principle, using osmotic pressure data, an energy scale for protein deformation can be obtained and the protein can be used as a biophysical probe in various environments. By placing a protein's structural deformation on a calibrated energy scale allows one to characterize and compare various environments. At a much different scale such an approach has been used to characterize the environment of amino acids using NMR spectroscopy [91].

Because of its larger size, and due to the possibility of anisotropic deformations, a test protein can offer some interesting applications. In our approach we essentially measure strain (deformation) under osmotic stress. This is accomplished by adding osmolytes such as polyethylene glycol (PEG) to the protein sample. In practice, any deformation force acts over a surface (as opposed to a single point) and therefore it is

appropriate to describe it as a pressure (force per unit area) or stress as in the context of material research. The resulting deformation under external stress is called strain. Stress-strain curves and Poisson's ratios that measure anisotropic deformations can provide a set of data that can be useful in material characterization. Deformation models can then be used in conjunction with the shape-dependent models that are currently used to fit scattering data as for example in Fig. 4.7 in this thesis. A shape affinity mapping can be created using the chi-squared reduced value from each fit. Such a combined approach can become a tool for describing possible transitions of shapes for a structure under study. The tool is still under development, but essentially it is a matrix of relative confidence levels from all possible (or most likely) shape models. The goals are to avoid assumptions that may lead to an incorrect or incomplete picture, to provide a landscape of the confidence levels for each potential model, to describe structures that fit more than one shape model in a way that is more representative of reality. Such an approach can be applied to other materials not just proteins.

6. CONCLUSIONS

In conclusion, we have shown that although scattering data from large protein aggregates such as A1AT and fibrinogen are difficult to analyze; by combining SAXS, SANS, and DLS methods we can obtain structural information that is otherwise inaccessible. Specifically, we have seen that osmotic stress can induce the aggregation of both A1AT and of fibrinogen. In the case of A1AT under osmotic stress we have identified two deformation regimes, namely a compression under lower stress values followed by abrupt aggregation at high stress. For fibrinogen we induced polymerization using the enzyme thrombin and measured characteristic scattering for fibrin networks. We then showed that high osmotic stress produces scattering curves similar to fibrin scattering.

REFERENCES

REFERENCES

- [1] N. E. Chayen, “Methods for separating nucleation and growth in protein crystallisation,” *Progress in Biophysics and Molecular Biology*, vol. 88, no. 3, pp. 329–337, 2005. [Online]. Available: <http://www.sciencedirect.com/science/article/pii/S0079610704000963>
- [2] A. McPherson, “Crystallization of proteins from polyethylene glycol,” *Journal of Biological Chemistry*, vol. 251, no. 20, pp. 6300–6303, 1976. [Online]. Available: <http://www.jbc.org/content/251/20/6300.abstract>
- [3] A. G. Kikhney and D. I. Svergun, “A practical guide to small angle x-ray scattering (saxs) of flexible and intrinsically disordered proteins,” *Febs Letters*, vol. 589, no. 19, pp. 2570–2577, 2015. [Online]. Available: Go to ISI://WOS:000362619600016
- [4] S. Antonysamy, Z. Bonday, R. M. Campbell, B. Doyle, Z. Druzina, T. Gheyi, B. Han, L. N. Jungheim, Y. Qian, C. Rauch, M. Russell, J. M. Sauder, S. R. Wasserman, K. Weichert, F. S. Willard, A. Zhang, and S. Emtage, “Crystal structure of the human prmt5:mep50 complex,” *Proceedings of the National Academy of Sciences*, vol. 109, no. 44, p. 17960, 2012. [Online]. Available: <http://www.pnas.org/content/109/44/17960.abstract>
- [5] S. H. Chen, “Small angle neutron scattering studies of the structure and interaction in micellar and microemulsion systems,” *Annual Review of Physical Chemistry*, vol. 37, pp. 351–399, 1986. [Online]. Available: <https://ui.adsabs.harvard.edu/abs/1986ARPC...37..351C>
- [6] D. I. Svergun, S. Richard, M. H. J. Koch, Z. Sayers, S. Kuprin, and G. Zaccai, “Protein hydration in solution: Experimental observation by x-ray and neutron scattering,” *Proceedings of the National Academy of Sciences*, vol. 95, no. 5, p. 2267, 1998. [Online]. Available: <http://www.pnas.org/content/95/5/2267.abstract>
- [7] H. D. T. Mertens and D. I. Svergun, “Structural characterization of proteins and complexes using small-angle x-ray solution scattering,” *Journal of Structural Biology*, vol. 172, no. 1, pp. 128–141, 2010. [Online]. Available: <http://www.sciencedirect.com/science/article/pii/S1047847710001905>
- [8] P. Bernadó, N. Shimizu, G. Zaccai, H. Kamikubo, and M. Sugiyama, “Solution scattering approaches to dynamical ordering in biomolecular systems,” *Biochimica Et Biophysica Acta-General Subjects*, vol. 1862, no. 2, pp. 253–274, 2018. [Online]. Available: Go to ISI://WOS:000423014400005
- [9] H. Dietz, F. Berkemeier, M. Bertz, and M. Rief, “Anisotropic deformation response of single protein molecules,” *Proceedings of the National Academy*

- of Sciences*, vol. 103, no. 34, p. 12724, 2006. [Online]. Available: <http://www.pnas.org/content/103/34/12724.abstract>
- [10] J. Gosline, M. Lillie, E. Carrington, P. Guerette, C. Ortlepp, and K. Savage, “Elastic proteins: biological roles and mechanical properties,” *Philosophical transactions of the Royal Society of London. Series B, Biological sciences*, vol. 357, no. 1418, pp. 121–132, 2002, 11911769[pmid] PMC1692928[pmcid]. [Online]. Available: <https://www.ncbi.nlm.nih.gov/pubmed/11911769> <https://www.ncbi.nlm.nih.gov/pmc/articles/PMC1692928/>
- [11] C. Storm, J. J. Pastore, F. C. MacKintosh, T. C. Lubensky, and P. A. Janmey, “Nonlinear elasticity in biological gels,” *Nature*, vol. 435, no. 7039, pp. 191–194, 2005. [Online]. Available: <https://doi.org/10.1038/nature03521>
- [12] I. Pogozheva, S. Tristram-Nagle, H. Mosberg, and A. Lomize, “Structural adaptation of proteins to different biological membranes,” *Biochimica et biophysica acta*, vol. 104, 2013.
- [13] H. I. Petrache, S. Tristram-Nagle, K. Gawrisch, D. Harries, V. A. Parsegian, and J. F. Nagle, “Structure and fluctuations of charged phosphatidylserine bilayers in the absence of salt,” *Biophysical Journal*, vol. 86, no. 3, pp. 1574–1586, 2004. [Online]. Available: <http://www.sciencedirect.com/science/article/pii/S0006349504742253>
- [14] K. G. DeFrates, R. Moore, J. Borgesi, G. Lin, T. Mulderig, V. Beachley, and X. Hu, “Protein-Based Fiber Materials in Medicine: A Review,” *NANOMATERIALS*, vol. 8, no. 7, JUL 2018.
- [15] E. Ban, H. Wang, J. M. Franklin, J. T. Liphardt, P. A. Janmey, and V. B. Shenoy, “Strong triaxial coupling and anomalous Poisson effect in collagen networks,” *PROCEEDINGS OF THE NATIONAL ACADEMY OF SCIENCES OF THE UNITED STATES OF AMERICA*, vol. 116, no. 14, pp. 6790–6799, APR 2 2019.
- [16] H. Zheng, C. Lu, J. Lan, S. Fan, V. Nanda, and F. Xu, “How electrostatic networks modulate specificity and stability of collagen,” *PROCEEDINGS OF THE NATIONAL ACADEMY OF SCIENCES OF THE UNITED STATES OF AMERICA*, vol. 115, no. 24, pp. 6207–6212, JUN 12 2018.
- [17] M. W. H. Kirkness, K. Lehmann, and N. R. Forde, “Mechanics and structural stability of the collagen triple helix,” *CURRENT OPINION IN CHEMICAL BIOLOGY*, vol. 53, pp. 98–105, DEC 2019.
- [18] H. Maiato and C. Ferras, “Actin divides to conquer,” *SCIENCE*, vol. 357, no. 6353, pp. 756–757, AUG 25 2017.
- [19] V. Roukos, “Actin proteins assemble to protect the genome,” *NATURE*, vol. 559, no. 7712, pp. 34–37, JUL 5 2018.
- [20] M.-F. Carlier and S. Shekhar, “Global treadmilling coordinates actin turnover and controls the size of actin networks,” *NATURE REVIEWS MOLECULAR CELL BIOLOGY*, vol. 18, no. 6, pp. 389–401, JUN 2017.
- [21] S. Eriksson, S. Janciauskiene, and L. Lannfelt, “Alpha 1-antichymotrypsin regulates alzheimer beta-amyloid peptide fibril formation,” *Proceedings of the National Academy of Sciences*, vol. 92, no. 6, p. 2313, 1995. [Online]. Available: <http://www.pnas.org/content/92/6/2313.abstract>

- [22] J. I. Guijarro, M. Sunde, J. A. Jones, I. D. Campbell, and C. M. Dobson, "Amyloid fibril formation by an sh3 domain," *Proceedings of the National Academy of Sciences*, vol. 95, no. 8, p. 4224, 1998. [Online]. Available: <http://www.pnas.org/content/95/8/4224.abstract>
- [23] A. Aggeli, I. A. Nyrkova, M. Bell, R. Harding, L. Carrick, T. C. McLeish, A. N. Semenov, and N. Boden, "Hierarchical self-assembly of chiral rod-like molecules as a model for peptide beta -sheet tapes, ribbons, fibrils, and fibers," *Proceedings of the National Academy of Sciences of the United States of America*, vol. 98, no. 21, pp. 11 857–11 862, 2001, 11592996[pmid] PMC59814[pmcid] 98/21/11857[PII]. [Online]. Available: <https://www.ncbi.nlm.nih.gov/pubmed/11592996>
<https://www.ncbi.nlm.nih.gov/pmc/articles/PMC59814/>
- [24] J. M. Alarcón, J. A. Brito, T. Hermosilla, I. Atwater, D. Mears, and E. Rojas, "Ion channel formation by alzheimer's disease amyloid β -peptide (a β 40) in unilamellar liposomes is determined by anionic phospholipids," *Peptides*, vol. 27, no. 1, pp. 95–104, 2006. [Online]. Available: <http://www.sciencedirect.com/science/article/pii/S0196978105003463>
- [25] F. Chiti and C. M. Dobson, "Protein misfolding, functional amyloid, and human disease," *Annual Review of Biochemistry*, vol. 75, no. 1, pp. 333–366, 2006. [Online]. Available: <https://doi.org/10.1146/annurev.biochem.75.101304.123901>
- [26] S. Devanathan, Z. Salamon, G. Lindblom, G. Gröbner, and G. o. Tollin, "Effects of sphingomyelin, cholesterol and zinc ions on the binding, insertion and aggregation of the amyloid a β 1-40 peptide in solid-supported lipid bilayers," *The FEBS Journal*, vol. 273, no. 7, pp. 1389–1402, 2006. [Online]. Available: <https://doi.org/10.1111/j.1742-4658.2006.05162.x>
- [27] R. Nelson, M. R. Sawaya, M. Balbirnie, A. v. Madsen, C. Riek, R. Grothe, and D. Eisenberg, "Structure of the cross-beta spine of amyloid-like fibrils," *Nature*, vol. 435, no. 7043, pp. 773–778, 2005, 15944695[pmid] PMC1479801[pmcid] nature03680[PII]. [Online]. Available: <https://www.ncbi.nlm.nih.gov/pubmed/15944695>
<https://www.ncbi.nlm.nih.gov/pmc/articles/PMC1479801/>
- [28] R. Nelson and D. Eisenberg, "Recent atomic models of amyloid fibril structure," *Current Opinion in Structural Biology*, vol. 16, no. 2, pp. 260–265, 2006. [Online]. Available: <http://www.sciencedirect.com/science/article/pii/S0959440X06000455>
- [29] M. R. R. de Planque, V. Raussens, S. A. Contera, D. T. S. Rijkers, R. M. J. Liskamp, J.-M. Ruysschaert, J. F. Ryan, F. Separovic, and A. Watts, " β -sheet structured β -amyloid(1-40) perturbs phosphatidylcholine model membranes," *Journal of Molecular Biology*, vol. 368, no. 4, pp. 982–997, 2007. [Online]. Available: <http://www.sciencedirect.com/science/article/pii/S0022283607002550>
- [30] S. J. Perkins, K. F. Smith, A. S. Nealis, P. I. Haris, D. Chapman, C. J. Bauer, and R. A. Harrison, "Secondary structure changes stabilize the reactive-centre cleaved form of serpins: A study by 1h nuclear magnetic resonance and fourier transform infrared spectroscopy," *Journal of Molecular Biology*, vol. 228, no. 4, pp. 1235–1254, 1992. [Online]. Available: <http://www.sciencedirect.com/science/article/pii/0022283692903291>

- [31] H. I. Petrache, A. Grossfield, K. R. MacKenzie, D. M. Engelman, and T. B. Woolf, "Modulation of glycophorin a transmembrane helix interactions by lipid bilayers: molecular dynamics calculations," *Journal of Molecular Biology*, vol. 302, no. 3, pp. 727–746, 2000. [Online]. Available: <http://www.sciencedirect.com/science/article/pii/S0022283600940725>
- [32] C. Fritz, B. Jeuck, C. Salas, R. Gonzalez, H. Jameel, and O. J. Rojas, "Nanocellulose and Proteins: Exploiting Their Interactions for Production, Immobilization, and Synthesis of Biocompatible Materials," in *CELLULOSE CHEMISTRY AND PROPERTIES: FIBERS, NANOCELLULOSES AND ADVANCED MATERIALS*, ser. Advances in Polymer Science, Rojas, OJ, Ed., 2016, vol. 271, pp. 207–224.
- [33] M. Mohsen-Nia and H. Modarress, "Association equation of state (aeos) based on aggregate formation for pure substance," *Chemical Physics*, vol. 336, no. 1, pp. 22–26, 2007. [Online]. Available: <http://www.sciencedirect.com/science/article/pii/S0301010406005593>
- [34] B. Vestergaard, M. Groenning, M. Roessle, J. S. Kastrup, M. van de Weert, J. M. Flink, S. Frokjaer, M. Gajhede, and D. I. Svergun, "A helical structural nucleus is the primary elongating unit of insulin amyloid fibrils," *PLoS biology*, vol. 5, no. 5, pp. e134–e134, 2007, 17472440[pmid] PMC1858711[pmcid] 06-PLBI-RA-1795R3[PII]. [Online]. Available: <https://www.ncbi.nlm.nih.gov/pubmed/17472440> <https://www.ncbi.nlm.nih.gov/pmc/articles/PMC1858711/>
- [35] M. Tashiro, M. Kojima, H. Kihara, K. Kasai, T. Kamiyoshihara, K. Ueda, and S. Shimotakahara, "Characterization of fibrillation process of α -synuclein at the initial stage," *Biochemical and Biophysical Research Communications*, vol. 369, no. 3, pp. 910–914, 2008. [Online]. Available: <http://www.sciencedirect.com/science/article/pii/S0006291X08003999>
- [36] H. Fukuda, A. Goto, and T. Imae, "Structure determination of helical fibers by numerical simulation for small-angle neutron scattering[†]," *Langmuir*, vol. 18, p. 7107, 2002.
- [37] C. Ricci, F. Spinozzi, P. Mariani, and M. G. Ortore, "Protein amyloidogenesis investigated by small angle scattering," *Current Pharmaceutical Design*, vol. 22, no. 26, pp. 3937–3949, 2016. [Online]. Available: Go to ISI://WOS:000384726200002
- [38] G. Massi, A. Fabiano, D. Ragusa, and P. Auconi, "Characterization of alpha-1-antitrypsin by isoelectric focusing on an ultrathin polyacrylamide gel layer," *Human Genetics*, vol. 53, no. 1, pp. 91–95, 1979. [Online]. Available: <https://doi.org/10.1007/BF00289456>
- [39] M. Brantly, T. Nukiwa, and R. G. Crystal, "Molecular basis of alpha-1-antitrypsin deficiency," *The American Journal of Medicine*, vol. 84, no. 6, Supplement 1, pp. 13–31, 1988. [Online]. Available: <http://www.sciencedirect.com/science/article/pii/0002934388901544>
- [40] K. F. Smith, R. A. Harrison, and S. J. Perkins, "Structural comparisons of the native and reactive-centre-cleaved forms of alpha 1-antitrypsin by neutron- and x-ray-scattering in solution," *The Biochemical journal*,

- vol. 267, no. 1, pp. 203–212, 1990, 2327980[pmid] PMC1131265[pmcid]. [Online]. Available: <https://www.ncbi.nlm.nih.gov/pubmed/2327980> <https://www.ncbi.nlm.nih.gov/pmc/articles/PMC1131265/>
- [41] P. R. Elliott, J.-P. Abrahams, and D. A. Lomas, “Wild-type α 1-antitrypsin is in the canonical inhibitory conformation,” *Journal of Molecular Biology*, vol. 275, no. 3, pp. 419–425, 1998. [Online]. Available: <http://www.sciencedirect.com/science/article/pii/S0022283697914583>
- [42] P. R. Elliott, X. Y. Pei, T. R. Dafforn, and D. A. Lomas, “Topography of a 2.0 Å structure of α 1-antitrypsin reveals targets for rational drug design to prevent conformational disease,” *Protein Science*, vol. 9, no. 7, pp. 1274–1281, 2000. [Online]. Available: <https://doi.org/10.1110/ps.9.7.1274>
- [43] S. Ye, A. L. Cech, R. Belmares, R. C. Bergstrom, Y. Tong, D. R. Corey, M. R. Kanost, and E. J. Goldsmith, “The structure of a michaelis serpin–protease complex,” *Nature Structural Biology*, vol. 8, no. 11, pp. 979–983, 2001. [Online]. Available: <https://doi.org/10.1038/nsb1101-979>
- [44] I. Petrache, I. Fijalkowska, T. R. Medler, J. Skirball, P. Cruz, L. Zhen, H. I. Petrache, T. R. Flotte, and R. M. Tudor, “ α -1 antitrypsin inhibits caspase-3 activity, preventing lung endothelial cell apoptosis,” *The American Journal of Pathology*, vol. 169, no. 4, pp. 1155–1166, 2006. [Online]. Available: <http://www.sciencedirect.com/science/article/pii/S0002944010625898>
- [45] R. M. Tudor and I. Petrache, “Molecular multitasking in the airspace: alpha1-antitrypsin takes on thrombin and plasmin,” *American journal of respiratory cell and molecular biology*, vol. 37, no. 2, pp. 130–134, 2007, 17541009[pmid] PMC1976548[pmcid] 2007-0163TR[PII]. [Online]. Available: <https://www.ncbi.nlm.nih.gov/pubmed/17541009> <https://www.ncbi.nlm.nih.gov/pmc/articles/PMC1976548/>
- [46] A. Lazrak, I. Nita, D. Subramaniam, S. Wei, W. Song, H.-L. Ji, S. Janciauskiene, and S. Matalon, “Alpha(1)-antitrypsin inhibits epithelial na⁺ transport in vitro and in vivo,” *American journal of respiratory cell and molecular biology*, vol. 41, no. 3, pp. 261–270, 2009, 19131639[pmid] PMC2742747[pmcid] 2008-0384OC[PII]. [Online]. Available: <https://www.ncbi.nlm.nih.gov/pubmed/19131639> <https://www.ncbi.nlm.nih.gov/pmc/articles/PMC2742747/>
- [47] G. B. Pott, E. D. Chan, C. A. Dinarello, and L. Shapiro, “ α 1-antitrypsin is an endogenous inhibitor of proinflammatory cytokine production in whole blood,” *Journal of Leukocyte Biology*, vol. 85, no. 5, pp. 886–895, 2009. [Online]. Available: <https://doi.org/10.1189/jlb.0208145>
- [48] A. D. Lockett, S. Kimani, G. Ddungu, S. Wrenger, R. M. Tudor, S. M. Janciauskiene, and I. Petrache, “ α 1-antitrypsin modulates lung endothelial cell inflammatory responses to tnf- α ,” *American journal of respiratory cell and molecular biology*, vol. 49, no. 1, pp. 143–150, 2013, 23526215[pmid] PMC3727880[pmcid] rcmb.2012-0515OC[PII]. [Online]. Available: <https://www.ncbi.nlm.nih.gov/pubmed/23526215> <https://www.ncbi.nlm.nih.gov/pmc/articles/PMC3727880/>

- [49] M. Kalfopoulos, K. Wetmore, and M. K. ElMallah, "Pathophysiology of Alpha-1 Antitrypsin Lung Disease," in *ALPHA-1 ANTITRYPSIN DEFICIENCY: METHODS AND PROTOCOLS*, ser. Methods in Molecular Biology, Borel, F and Mueller, C, Ed., 2017, vol. 1639, pp. 9–19.
- [50] S. Santangelo, S. Scarlata, M. L. Poeta, A. J. Bialas, G. Paone, and R. A. Incalzi, "Alpha-1 Antitrypsin Deficiency: Current Perspective from Genetics to Diagnosis and Therapeutic Approaches," *CURRENT MEDICINAL CHEMISTRY*, vol. 24, no. 1, pp. 65–90, 2017.
- [51] J. H. Teckman and K. S. Blomenkamp, "Pathophysiology of Alpha-1 Antitrypsin Deficiency Liver Disease," in *ALPHA-1 ANTITRYPSIN DEFICIENCY: METHODS AND PROTOCOLS*, ser. Methods in Molecular Biology, Borel, F and Mueller, C, Ed., 2017, vol. 1639, pp. 1–8.
- [52] K. Lederer, "Small angle x-ray scattering measurements with dilute solutions of bovine fibrinogen," *Journal of Molecular Biology*, vol. 63, no. 2, pp. 315–320, 1972. [Online]. Available: <http://www.sciencedirect.com/science/article/pii/0022283672903786>
- [53] G. Marguerie and H. B. Stuhmann, "A neutron small-angle scattering study of bovine fibrinogen," *Journal of Molecular Biology*, vol. 102, no. 1, pp. 143–156, 1976. [Online]. Available: <http://www.sciencedirect.com/science/article/pii/0022283676900784>
- [54] G. Dietler, W. Kaenzig, A. Haeberli, and P. W. Straub, "Temperature dependence of fibrin polymerization: a light scattering study," *Biochemistry*, vol. 24, no. 23, pp. 6701–6706, 1985. [Online]. Available: <https://doi.org/10.1021/bi00344a060>
- [55] H. C. F. Côté, S. T. Lord, and K. P. Pratt, " γ -chain dysfibrinogenemias: Molecular structure-function relationships of naturally occurring mutations in the γ chain of human fibrinogen," *Blood*, vol. 92, no. 7, pp. 2195–2212, 1998. [Online]. Available: <https://doi.org/10.1182/blood.V92.7.2195>
- [56] R. F. Doolittle, "Structural basis of the fibrinogen–fibrin transformation: contributions from x-ray crystallography," *Blood Reviews*, vol. 17, no. 1, pp. 33–41, 2003. [Online]. Available: <http://www.sciencedirect.com/science/article/pii/S0268960X02000607>
- [57] W. Li, D. J. D. Johnson, T. E. Adams, N. Pozzi, V. De Filippis, and J. A. Huntington, "Thrombin inhibition by serpins disrupts exosite ii," *The Journal of biological chemistry*, vol. 285, no. 49, pp. 38 621–38 629, 2010, 20889971[pmid] PMC2992294[pmcid] M110.144964[PII]. [Online]. Available: <https://www.ncbi.nlm.nih.gov/pubmed/20889971> <https://www.ncbi.nlm.nih.gov/pmc/articles/PMC2992294/>
- [58] L.-D. Koh, J. Yeo, Y. Y. Lee, Q. Ong, M. Han, and B. C.-K. Tee, "Advancing the frontiers of silk fibroin protein-based materials for futuristic electronics and clinical wound-healing," *MATERIALS SCIENCE & ENGINEERING C-MATERIALS FOR BIOLOGICAL APPLICATIONS*, vol. 86, pp. 151–172, MAY 1 2018.

- [59] S. Hollingshead, C.-Y. Lin, and J. C. Liu, "Designing Smart Materials with Recombinant Proteins," *MACROMOLECULAR BIOSCIENCE*, vol. 17, no. 7, JUL 2017.
- [60] H. Sun, Q. Luo, C. Hou, and J. Liu, "Nanostructures based on protein self-assembly: From hierarchical construction to bioinspired materials," *NANO TODAY*, vol. 14, pp. 16–41, JUN 2017.
- [61] M. Supova, "The Significance and Utilisation of Biomimetic and Bioinspired Strategies in the Field of Biomedical Material Engineering: The Case of Calcium Phosphate-Protein Template Constructs," *MATERIALS*, vol. 13, no. 2, JAN 2 2020.
- [62] Y. Wang, P. Katyal, and J. K. Montclare, "Protein-Engineered Functional Materials," *ADVANCED HEALTHCARE MATERIALS*, vol. 8, no. 11, JUN 2019.
- [63] J. S. Evans, "Composite Materials Design: Biom mineralization Proteins and the Guided Assembly and Organization of Biom mineral Nanoparticles," *MATERIALS*, vol. 12, no. 4, FEB 2 2019.
- [64] K. Szalapata, M. Osinska-Jaroszuk, J. Kapral-Piotrowska, B. Pawlikowska-Pawlega, R. Lopucki, R. Mrocza, and A. Jarosz-Wilkolazka, "Serine Protease Inhibitors-New Molecules for Modification of Polymeric Biomaterials," *BIOMOLECULES*, vol. 10, no. 1, JAN 2020.
- [65] M. C. Diaz, P. J. Hall, C. E. Snape, S. D. Brown, and R. Hughes, "Contrast-matching small-angle neutron scattering to monitor the accessibility of solvents to the porosity of coked fcc catalysts," *Industrial & Engineering Chemistry Research*, vol. 41, no. 25, pp. 6566–6571, 2002. [Online]. Available: <https://doi.org/10.1021/ie000868y>
- [66] P. Bernadó, E. Mylonas, M. V. Petoukhov, M. Blackledge, and D. I. Svergun, "Structural characterization of flexible proteins using small-angle x-ray scattering," *Journal of the American Chemical Society*, vol. 129, no. 17, pp. 5656–5664, 2007. [Online]. Available: <https://doi.org/10.1021/ja069124n>
- [67] C. Stanley, S. Krueger, V. A. Parsegian, and D. C. Rau, "Protein structure and hydration probed by sans and osmotic stress," *Biophysical journal*, vol. 94, no. 7, pp. 2777–2789, 2008, 18178651[pmid] PMC2267150[pmcid] S0006-3495(08)70529-0[PII]. [Online]. Available: <https://www.ncbi.nlm.nih.gov/pubmed/18178651>
<https://www.ncbi.nlm.nih.gov/pmc/articles/PMC2267150/>
- [68] A. Rekas, V. Lo, G. E. Gadd, R. Cappai, and S. I. Yun, "Pamam dendrimers as potential agents against fibrillation of α -synuclein, a parkinson's disease-related protein," *Macromolecular Bioscience*, vol. 9, no. 3, pp. 230–238, 2009. [Online]. Available: <https://doi.org/10.1002/mabi.200800242>
- [69] J. Curtis, A. McAuley, H. Nanda, and S. Krueger, "Protein structure and interactions in the solid state studied by small-angle neutron scattering," *Faraday discussions*, vol. 158, pp. 285–99; discussion 351, 2012.
- [70] R. P. Rambo and J. A. Tainer, *Super-Resolution in Solution X-Ray Scattering and Its Applications to Structural Systems Biology*, ser. Annual Review of Biophysics. Annual Reviews, 2013, vol. 42, pp. 415–441. [Online]. Available: [Go to ISI://WOS:000321695700019](https://doi.org/10.1146/annurev-biophys-070312-103731)

- [71] F. Gabel, *Small-Angle Neutron Scattering for Structural Biology of Protein-RNA Complexes*, ser. Methods in Enzymology. Academic Press, 2015, vol. 558, pp. 391–415. [Online]. Available: [Go to ISI://WOS:000405656400014](https://doi.org/10.1016/B978-0-12-405656-4.00014)
- [72] N. R. Zaccai, C. W. Sandlin, J. T. Hoopes, J. E. Curtis, P. J. Fleming, K. G. Fleming, and S. Krueger, *Deuterium Labeling Together with Contrast Variation Small-Angle Neutron Scattering Suggests How Skp Captures and Releases Unfolded Outer Membrane Proteins*, ser. Methods in Enzymology. Academic Press, 2016, vol. 566, pp. 159–210. [Online]. Available: [Go to ISI://WOS:000410545400007](https://doi.org/10.1016/B978-0-12-410545-4.00007)
- [73] D. H. Perlmutter, “alpha 1-antitrypsin Deficiency: A Misfolded Secretory Protein Variant with Unique Effects on the Endoplasmic Reticulum,” *ENDOPLASMIC RETICULUM STRESS IN DISEASES*, vol. 3, no. 1, pp. 63–72, JAN 2016.
- [74] F. Szoka, “Comparative Properties and Methods of Preparation of Lipid Vesicles (Liposomes),” *Ann. Rev. Biophys. Bioeng.*, vol. 9, no. , pp. 467–517, 1980.
- [75] M. Ballauff, “Analysis of Polymer Colloids by Small-Angle X-Ray and Neutron Scattering: Contrast Variation,” *ADVANCED ENGINEERING MATERIALS*, vol. 13, no. 8, SI, pp. 793–802, AUG 2011.
- [76] S. J. Perkins, K. F. Smith, J. M. Kilpatrick, J. E. Volanakis, and R. B. Sim, “Modelling of the serine-proteinase fold by x-ray and neutron scattering and sedimentation analyses: occurrence of the fold in factor d of the complement system,” *The Biochemical journal*, vol. 295 (Pt 1), no. Pt 1, pp. 87–99, 1993, 8216242[pmid] PMC1134824[pmcid]. [Online]. Available: <https://www.ncbi.nlm.nih.gov/pubmed/8216242>
<https://www.ncbi.nlm.nih.gov/pmc/articles/PMC1134824/>
- [77] Y. M. Efimova, A. A. van Well, U. Hanefeld, B. Wierczinski, and W. G. Bouwman, “On the neutron scattering length density of proteins in h₂o/d₂o,” *Physica B: Condensed Matter*, vol. 350, no. 1, Supplement, pp. E877–E880, 2004. [Online]. Available: <http://www.sciencedirect.com/science/article/pii/S092145260400451X>
- [78] N. L. Abbott, D. Blankschtein, and T. A. Hatton, “Protein partitioning in two-phase aqueous polymer systems. 4. proteins in solutions of entangled polymers,” *Macromolecules*, vol. 25, no. 20, pp. 5192–5200, 1992. [Online]. Available: <https://doi.org/10.1021/ma00046a013>
- [79] V. A. Parsegian, R. P. Rand, and D. C. Rau, “Osmotic stress, crowding, preferential hydration, and binding: A comparison of perspectives,” *Proceedings of the National Academy of Sciences of the United States of America*, vol. 97, no. 8, pp. 3987–3992, 2000, 10760270[pmid] PMC18129[pmcid] 97/8/3987[PII]. [Online]. Available: <https://www.ncbi.nlm.nih.gov/pubmed/10760270>
<https://www.ncbi.nlm.nih.gov/pmc/articles/PMC18129/>
- [80] M. A. Johnson, S. Seifert, H. I. Petrache, and A. C. Kimbe-Hill, “Phase Coexistence in Single-Lipid Membranes Induced by Buffering Agents,” *LANGMUIR*, vol. 30, no. 33, pp. 9880–9885, AUG 26 2014.
- [81] X. Garcia, L. Seyve, Z. Tellier, G. Chevreux, N. Bihoreau, B. Polack, and F. Caton, “Aggregates Dramatically Alter Fibrin Ultrastructure,” *BIOPHYSICAL JOURNAL*, vol. 118, no. 1, pp. 172–181, JAN 7 2020.

- [82] P. Zeliszewska, M. Sadowska, M. Morga, and Z. Adamczyk, "Mechanism of fibrinogen /microparticle complex deposition on solid substrates: Role of pH," *COLLOIDS AND SURFACES B-BIOINTERFACES*, vol. 184, DEC 1 2019.
- [83] B. Haemisch, A. Buengeler, C. Kielar, A. Keller, O. Strube, and K. Huber, "Self-Assembly of Fibrinogen in Aqueous, Thrombin-Free Solutions of Variable Ionic Strengths," *LANGMUIR*, vol. 35, no. 37, pp. 12 113–12 122, SEP 17 2019.
- [84] S. Yesudasan, X. Wang, and R. D. Averett, "Fibrin polymerization simulation using a reactive dissipative particle dynamics method," *BIOMECHANICS AND MODELING IN MECHANOBIOLOGY*, vol. 17, no. 5, pp. 1389–1403, OCT 2018.
- [85] B. M. Scott and W. P. Sheffield, "Engineering the serpin alpha(1)-antitrypsin: A diversity of goals and techniques," *PROTEIN SCIENCE*, vol. 29, no. 4, pp. 856–871, APR 2020.
- [86] A. Lucas, J. R. Yaron, L. Zhang, C. Macaulay, and G. McFadden, "Serpins: Development for Therapeutic Applications," in *SERPINS: METHODS AND PROTOCOLS*, ser. Methods in Molecular Biology, Lucas, A, Ed., 2018, vol. 1826, pp. 255–265.
- [87] S. Krishnan, H. J. Whitwell, J. Cuenco, A. Gentry-Maharaj, U. Menon, S. P. Pereira, M. Gaspari, and J. F. Timms, "Evidence of Altered Glycosylation of Serum Proteins Prior to Pancreatic Cancer Diagnosis," *INTERNATIONAL JOURNAL OF MOLECULAR SCIENCES*, vol. 18, no. 12, DEC 2017.
- [88] A. D. Lockett, "Alpha-1 Antitrypsin Transcytosis and Secretion," in *ALPHA-1 ANTITRYPSIN DEFICIENCY: METHODS AND PROTOCOLS*, ser. Methods in Molecular Biology, Borel, F and Mueller, C, Ed., 2017, vol. 1639, pp. 173–184.
- [89] N. Hadzic, "Therapeutic Options in Alpha-1 Antitrypsin Deficiency: Liver Transplantation," in *ALPHA-1 ANTITRYPSIN DEFICIENCY: METHODS AND PROTOCOLS*, ser. Methods in Molecular Biology, Borel, F and Mueller, C, Ed., 2017, vol. 1639, pp. 263–265.
- [90] A. M. Gruntman and T. R. Flotte, "Therapeutics: Gene Therapy for Alpha-1 Antitrypsin Deficiency," in *ALPHA-1 ANTITRYPSIN DEFICIENCY: METHODS AND PROTOCOLS*, ser. Methods in Molecular Biology, Borel, F and Mueller, C, Ed., 2017, vol. 1639, pp. 267–275.
- [91] M. A. Johnson, B. D. Ray, S. R. Wassall, and H. I. Petrache, "Equivalent Iso-propanol Concentrations of Aromatic Amino Acids Interactions with Lipid Vesicles," *JOURNAL OF MEMBRANE BIOLOGY*, vol. 248, no. 4, pp. 695–703, AUG 2015.

VITA

VITA

Luis A. Palacio, P.E.

EDUCATION

2009 – present	Ph.D. student	Physics, Purdue University, Indianapolis
2004 - 2007	M.S.	Physics, Purdue University, Indianapolis
2001 - 2004	B.S.	Physics, Purdue University, Fort Wayne
1993 - 1999	B.S.	Mechanical Engineering (Cum Laude), University of Puerto Rico, Mayagüez

RECENT POSITIONS

10/2015–Present Executive Director / CEO, Health and Science Innovations, Inc. (Indianapolis, IN)

Description: Provide leadership; set policies, standards, and procedures; continually develop the organization; develop resources and seek external funding; design, plan and execute educational programs; provide direct mentorship to students; manage the portfolio of research projects and labs; oversee payroll, human resources, marketing, and financial operations; continuously engage the community; and generate outcome/business reports.

08/2009–Present Research Assistant, Department of Physics, Indiana University-Purdue University (Indianapolis, IN)

Description: Design and execute experiments using X-rays and Neutron Scattering techniques, write research proposals for experiments at National Laboratories, supervise and mentor students, perform maintenance and mechanical repairs of laboratory instruments. Use computational methods to analyze data and model systems

under study. Present research findings at conferences, and publish in peer-reviewed journals.

10/2013–12/2016 Secretary of the Board of Directors, Health and Science Innovations, Inc. (Indianapolis, IN)

Description: Responsible for ensuring that accurate and sufficient documentation exists to meet legal requirements, and make them available when required by authorized persons.

10/2013–12/2016 Director of Research and Development, Alivio Medical Center (Indianapolis, IN)

Description: Manage, coordinate, provide direction and conduct science and engineering research, medical products development and clinical research. Secure funding and resources for research and projects by writing grant proposals and developing partnerships with other institutions. Review protocols and verify compliance with regulations.

SKILLS

- Fluent in English & Spanish. Learning German, French, and Russian.
- Effective analytical, problem solving and investigative skills, including failure analysis.
- Excellent communication skills and ability to work collaboratively with business partners and with cross-functional teams.
- Agile learner, innovative, strategic thinker, and highly adaptable to different operation phases or modes.
- Ability to develop in-depth business and product knowledge, and strong relationships with business partners.
- Broad technical skills and experience with the following programming tools: C/C++, MS Access, Perl, Python, UNIX, Shell, HTML, and MATLAB.

- Small Angle X-ray and Neutron Scattering techniques and analysis of proteins and lipid membranes in solution.
- Light Scattering techniques for elucidating size and charge of nano-micro molecules in solution.
- Electrophysiology measurements and analysis of ion channels on lipid bi-layers.

PRODUCTS AND SOLUTIONS

- Author and Co-Founder of the IDEAA (Innovation, Design, Engineering, Advanced-Manufacturing, and Automation) workforce development initiative for the state of Indiana, to develop a comprehensive talent pipeline and support network that connects job-seekers to employers with operations in IDEAA fields.
- Author and Co-Founder of the Tech Literacy program for 3rd to 8th graders.
- Secured over \$3M in funding and resources for Health & Science Innovations over 5 years.
- Created the award winning Tech Literacy Program to help undeserved kids learn tech skills.
- Designed a 2,000 sq-ft biotechnology / engineering laboratory and managed the construction.
- Designed and developed a dynamic database for Physical Therapy to track progress of patients.
- Researched and developed a human fall detection logic for a wearable device.
- Designed a novel coupling disk as part of a mechanism aimed at immediately stopping reverse rotation of a vertical electric motor in sewer and pumping operations during power outage.
- Designed and created a global database system in MS Access to schedule and track customer and engineering test requests of AC Industrial Motors built by

General Electric. This software served manufacturing and engineering centers in the USA, Canada, Mexico, India, China, Brazil.

- Created and managed a new Center for Bearing Failure Analysis within GE Power Conversion to reduce warranty cost, and improve quality and customer satisfaction.
- Designed and created a Bearing Life Calculator tool to aid global engineering design teams in the selection of bearings for AC Industrial Motors.

EXPERIENCE:

10/2013–10/2015 Director of Programs and Research, Health and Science Innovations, Inc. (Indianapolis, IN)

Description: Manage, coordinate, provide direction and conduct science and engineering research, medical products development and clinical research. Secure funding and resources for research and projects by writing grant proposals and developing partnerships with other institutions. Review protocols and verify compliance with regulations. Plan and coordinate the Young Innovators Quest (STEM) program for high school students.

04/2012–05/2013 Professional Engineer Consultant, Uncommon Engineering (Indianapolis, IN)

Description: Provided direct advice and engineering consulting services to the CEO of Uncommon Engineering. Reviewed the thermodynamic design of his new, patented based, hybrid thermal-electric engine system.

06/2011–05/2013 National Science Foundation GK-12 Fellow, Southport High School (Indianapolis, IN)

Description: Worked directly with High School Physics and Engineering teachers (15 hrs./week) to develop and co-teach age-appropriate, hands-on classroom lessons and activities that were broadly related to the NSF Fellow's area of research.

08/2009–05/2010 Teaching Assistant, Department of Physics, Indiana University-Purdue University (Indianapolis, IN)

Description: In charge of teaching introductory physics mechanics laboratory to college students. Taught over 190 students, managed the classroom, created assignments, and graded lab reports.

08/2004–12/2007 Theoretical and Computational Biophysics Research Assistant, Department of Physics, Indiana University-Purdue University (Indianapolis, IN)

Description: Conducted protein folding research by designing and executing experiments that tested how Statistical Mechanics principles apply to the process of protein folding states. Translated research questions into mathematical models that were programmed into C++ simulations. Collected and analyzed data to produce results that led to the M.S. thesis.

04/2000–08/2004 Applications & Design Engineer, General Electric (GE) Consumer and Industrial (Fort Wayne, Indiana)

Description: Designed custom AC induction motors to meet customer specifications and assure industry standards compliance. Worked with GE Global Engineering Team to provide leadership for mechanical design, product application and projects. Provided engineering support to Marketing, Manufacturing, Warranty, and Sales teams.

07/2005–07/2005 Volunteer Medical and Dental Assistant, Ministry International (Arequipa, Perú S.A.)

Description: Helped with set up of ambulatory clinics in underserved communities of Arequipa, Perú, and serve as an interpreter between medical doctors or dentists, and patients.

06/1998–01/2000 Administrative Assistant, PR Transportation Technology Transfer Center (Mayagüez, PR)

Description: This center is a federally sponsored organization with the mission of educating civil engineering firms and local government agencies on current Federal

Transportation standards and guidelines. I worked developing a database to manage seminars and events, provided technical support to the office, and as a publications editor.

08/1999–12/1999 Manufacturing Consultant, Hewlett Packard, Puerto Rico (Aguadilla, Puerto Rico)

Description: Contracted to design a system able to maintain the tracks of the ink-jet cartridge production line clean after ink spills.

08/1998–01/2000 Retail Associate

10/1994–08/1997 Marshalls, Inc (Mayagüez, Puerto Rico)

Description: Sales clerk, stockroom clerk, cashier and customer service desk.

CONSULTING

- VoCare CEO (Steve Peabody) on matters of fall detection for wireless medical devices.
- CreateIT CEO (Jamie Schnitzius) on matters of mobile medical translation system development for Hispanic and minority patients of Alivio Medical Center.
- MedDiary CEO (Mark Repko) on matters of mobile medical App development for diabetic patients of Alivio Medical Center.
- NIH Bezrukov Lab Staff Scientist (Tatiana K. Rostovtseva) on matters of nanoparticles sizing.
- Dr. Elliot Rosen (IU School of Medicine) on matters of microfluidics for blood clotting studies.

PEER REVIEWED ARTICLES

A. Lopez-Yunez, D. Vasquez, **L.A. Palacio**, N. Tiwari, V.K. Survaqdevara, M. Anandwala, and M. Rizkalla, (2014) A Novel Approach for High Speed Wireless Pre-Fall Detection Multisensory System. IEEE 57th International Midwest Symposium

on Circuits and Systems Proceedings: 857-859.

M.M. Koerner, **L.A. Palacio**, J.W. Wright, K.S. Schweitzer, B.D. Ray, H.I. Petrache, (2011) Electrodynamics of Lipid Membrane Interactions in the Presence of Zwitterionic Buffers. *Biophysical Journal* 101 (2): 362-369.

CONFERENCE ABSTRACTS

T.N. Segally, **L.A. Palacio**, J. Kim, C.B. Stanley, S. Seifert, H.I. Petrache. (2018) Differentiating Structural Changes of Glycoproteins in Solution using Small Angle Scattering Analysis, Vol. 116, (3): 474a.

L.A. Palacio, C.B. Stanley, L. Burke, R.Lybarger, H.I. Petrache. (2016) Small Angle Neutron Scattering of Fibrinogen Polymerization Kinetics. *Biophysical Journal*, Vol. 110, (3): 385a.

L.A. Palacio, C.B. Stanley, L. Burke, R.Lybarger, H.I. Petrache. (2016) Small Angle Neutron Scattering of Fibrinogen Polymerization Kinetics. *Biophysical Journal*, Vol. 110, (3): 385a.

L.A. Palacio, C.B. Stanley, S. Seifert, R.Lybarger, H.I. Petrache. (2015) Small Angle Neutron and X-Ray Scattering of Plasma Glycoprotein Interactions with Lipid Membranes. *Biophysical Journal*, Vol. 108, (2): 516a.

G. Figueroa, **L.A. Palacio**, B.D. Ray, H.I. Petrache, A. Lopez-Yunez. (2015) Detecting Counterfeit Pharmaceuticals through UV Spectrophotometry. *Biophysical Journal*, Vol. 108, (2): 622a.

L.A. Palacio, C.B. Stanley, S. Seifert, H.I. Petrache. (2014) Small Angle Scattering of Fibrinogen Polymerization Kinetics and of Alpha1 Antitrypsin Interactions

with Lipid Membranes. *Biophysical Journal*, Vol. 106 (2): 301a.

P. Srinivasan, R. Kumar, **L.A. Palacio**, H.I. Petrache. (2014) Statistics of Simulated Ion Channels *Biophysical Journal*, Vol. 106 (2): 558a–559a.

J.J. Kinnun, K.J. Mallikarjunaiah, **L.A. Palacio**, M.F. Brown, H.I. Petrache. (2014) Intermembrane Forces and Membrane Deformation Observed via Dehydration and Osmotic Pressure. *Biophysical Journal*, Vol. 106 (2): 287a.

L.A. Palacio, C.B. Stanley, A.K. Fraser, M.A. Johnson, H.I. Petrache. (2013) Structural Changes of Alpha1-Antitrypsin Under Osmotic Pressure and in the Presence of Lipid Membranes. *Biophysical Journal* 104 (2): 595a-596a.

J.J. Kinnun, K.J. Mallikarjunaiah, **L.A. Palacio**, M.F. Brown, H.I. Petrache. (2013) Membrane Structure and Intermembrane Forces Observed with Small Angle X-Ray Scattering. *Biophysical Journal* 104 (2): 81a.

L.A. Palacio, H.I. Petrache. (2012) Analysis of Multichannel Signals using a Channel Simulator. *Biophysical Journal* 102 (3): 683a.

T.C. Roark, **L.A. Palacio**, P.A. Gurnev, B.D. Ray, H.I. Petrache. (2012) Interactions of Lithium Ions with Lipid Membranes. *Biophysical Journal* 102 (3): 96a.

J.W. Wright, M.M. Koerner, R.Z. Lybarger, **L.A. Palacio**, H.I. Petrache. (2012) Partitioning of Solutes in Lipid Multilayers. *Biophysical Journal* 102 (3): 97a.

R.Z. Lybarger, J.W. Wright, **L.A. Palacio**, K. Szymanski, H.I. Petrache. (2012) Measurements of Solute Polarizabilities Affecting Lipid Membrane Interactions. *Biophysical Journal* 102 (3): 334a–335a.

L.A. Palacio, P. DeMoss, H.I. Petrache. (2011) Analysis of Glycoprotein Interactions with Multichannel Membranes. *Biophysical Journal* 100(3): 638a.

K.J. Mallikarjunaiah, J.J. Kinnun, A.Leftin, **L.A. Palacio**, M.J. Justice, H.I. Petrache, M.F. Brown. (2011) Area Deformation of Membranes from the Perspective of 2H NMR and X-ray Scattering. *Biophysical Journal* 100 (3): 173a.

ORAL PRESENTATIONS

L.A. Palacio. (2016) Proposal for “IDEAA-Manufacturing Partnership” to the Indiana Dept. of Workforce Development. Region 5 Works Council (Indianapolis, IN).

L.A. Palacio, C.B. Stanley, S. Seifert, R. Lybarger, H.I. Petrache. (2014) Small Angle Scattering of Fibrinogen Polymerization Kinetics and of Alpha1 Antitrypsin Interactions with Lipid Membranes. Indiana Academy of Science 129th Annual Meeting (Indianapolis, IN).

L.A. Palacio and J. Adler. (2013) Project-Based Learning and Partnerships: Blending Curriculum with Career Skills. International Teacher Scientist Partnership Conference (Boston, MA).

L.A. Palacio, Horia I. Petrache. (2013) Structural Changes of Alpha 1-Antitrypsin under Osmotic Pressure and in the Presence of Lipid Membranes. Indiana Academy of Science 128th Annual Academy Meeting (Indianapolis, IN).

PRESS & MEDIA

Promising Practice: Health and Science Innovations'Young Innovators Quest Program; Indiana Pathways Innovation Network; August, 2016. Preparing the Next Generation of Innovators. Embrace Diversity Magazine; Fall 2015, p. 4.

Ph.D. Physics Student Urges Members of Congress to Support Science and Technology Research. Inside IUPUI Editor's Pick; July 9, 2013.

STEM Fellows: Science Grad Students Promote Science to Local Students. Indianapolis Star; June 4, 2012, front page.

ADDITIONAL TRAINING

- Indiana Professional Engineering License, PE10606511 (2006 - Present).
- Neutrons in Biology, by ORNL and North Carolina State University (2016).
- Frontiers in Neutron Structural Biology, by Oak Ridge National Laboratories (2013).
- Presentation Boot Camp Workshop, by Dr. Richard Tankersley (2012).
- Social/Behavioral Researchers, Human Research 2 Curriculum, by the Collaborative Institutional Training Initiative (2012), for Internal Review Board investigator approval.
- Lubrication Analysis for Bearings (2003).
- Vibration Analysis of Rotating Machinery (2003).
- ANSYS Introductory Course by GE Canada (2003).
- Bearing Selection, Design and Failure Analysis (2002).
- Six Sigma Methodology; Green Belt certified by GE (2001); last project completed in Feb. 2016.

ACADEMIC EXPERIENCE

01/2009–Present Ion Channels and Lipid Membrane Structure

Use physical methods to study the structural parameters of lipid membranes and how these membranes interact with proteins of interest under different conditions. Methods include: small angle x-ray scattering, neutron scattering, lipid bi-layer ion channel current measurements, light scattering, zeta-potential measurements and microfluidic devices.

01/2006–12/2007 Protein Knowledge Based Potential (M.S. Thesis)

Used computational methods to study how to improve protein knowledge based potentials for coarse grained models by testing traditional fundamental assumptions like the application of the Boltzmann distribution to amino acids pairwise distances of crystallized proteins in order to extract pairwise potentials and predict protein folding.

01/2004–05/2004 Resonance

Studied the resonance phenomenon through research and experimentation of mechanical vibration, RLC circuit resonance and electron spin resonance.

08/2003–12/2003 Atomic and Molecular Spectroscopy

Studied spectroscopy through research and experimentation. Created a digital spectrograph able to measure relative intensity and wavelengths of a given line spectrum.

08/1999–12/1999 Finite Element Analysis

CAD structural analysis project. Created a program in Matlab able to calculate the strains and stresses of a given solid structure.

01/1998–05/1998 House Construction based on Heating and Cooling Load HVAC design project

Calculated the heating and cooling loads, and selected construction materials for a given house plan located in Indiana.

01/1998–05/1998 Catamaran Hull Outboard Motor Redesign

Fluid mechanics project. Investigated the cause of poor propeller performance of a Harris Kayot catamaran boat, suggested possible solutions, and built a prototype.

SELECTED AWARDS

- United Way (UWCI) IMPACT in Education Awards for Tech Literacy, 2018.
- Skill UP 3 Indiana Workforce Development Grant (\$931k), 2018.
- Skill UP 2 Indiana Workforce Development Grant (\$532k), 2016.
- Nominee for AAAS/Science Program for Excellence in Science, 2016–2018.
- Five beam time awards for experiments at EQ-SANS (BL6), Oak Ridge National Laboratory (ORNL), 2011–2014.
- National Science Foundation GK-12 Fellowship, 2011–2013.
- Southern Regional Education Board Dissertation Scholar, 2011–2013.
- Indiana University Research Investment Fund Fellowship, 2004–2005.

IMPACT & MENTORING:

- 600 Elementary school students learning tech, or working on science fair projects.
- 240 High school students through STEM Programs.
- 190 Undergraduate students in physics (mechanics) labs, and 4 preparing for the MCAT.
- 19 Science and engineering undergraduate students working in various research projects.
- 3 Undergraduate engineering students at General Electrical (COOP).
- 2 Electrical Engineering graduate students working on biomedical communications systems.
- 1 Physics Post-Doc at Oak Ridge National Laboratory.

COMMUNITY ENGAGEMENT

- Advocacy for importance of scientific research to U.S. Congress members
- IUPUI, School of Science Diversity Council
- Marian University Hispanic Advisory Board
- Indiana After-school Network STEM Taskforce
- Indiana Senate Latino Roundtable
- Science Olympiad IUPUI Invitational Master of Ceremony
- 2016 Central Indiana Regional Science and Engineering Fair Judge
- Gleaners Food Bank of Indiana Volunteer
- Million Meals Marathon Indianapolis Volunteer

MEMBERSHIP, BOARDS AND COMMITTEES

- Society of Hispanic Professional Engineers (SHPE); Co-chair of SHPE Jr., Indiana Chapter
- Indiana Academy of Science; Member of Membership Advisory Committee
- Biophysical Society
- American Association for the Advancement of Science (AAAS)
- National User Facility Organization (NUFO)
- American Physical Society (APS)
- National Society of Hispanic Physicists (NSHP)
- National Science Teachers Association (NSTA)